



**HAL**  
open science

## Tectonic inversion of an asymmetric graben: insights from a combined field and gravity survey in the Sorbas basin

Damien Do Couto, Charles Gumiaux, Romain Augier, Noémie Lebret, Nicolas Folcher, Gwenael Jouannic, Laurent Jolivet, Jean-Pierre Suc, Christian Gorini

### ► To cite this version:

Damien Do Couto, Charles Gumiaux, Romain Augier, Noémie Lebret, Nicolas Folcher, et al.. Tectonic inversion of an asymmetric graben: insights from a combined field and gravity survey in the Sorbas basin. *Tectonics*, 2014, 33 (7), pp.1360-1385. 10.1002/2013TC003458 . insu-01017447

**HAL Id: insu-01017447**

**<https://insu.hal.science/insu-01017447>**

Submitted on 30 Jul 2014

**HAL** is a multi-disciplinary open access archive for the deposit and dissemination of scientific research documents, whether they are published or not. The documents may come from teaching and research institutions in France or abroad, or from public or private research centers.

L'archive ouverte pluridisciplinaire **HAL**, est destinée au dépôt et à la diffusion de documents scientifiques de niveau recherche, publiés ou non, émanant des établissements d'enseignement et de recherche français ou étrangers, des laboratoires publics ou privés.



## Tectonics

### RESEARCH ARTICLE

10.1002/2013TC003458

#### Key Points:

- The Sorbas basin shows a strong asymmetric structure
- The basin has been initiated during an extensional regime
- It then experienced a severe N-S oriented tectonic inversion from 8 Ma

#### Correspondence to:

D. Do Couto  
damien.docouto@unige.ch

#### Citation:

Do Couto, D., C. Gumiaux, R. Augier, N. Le Bret, N. Folcher, G. Jouannic, L. Jolivet, J.-P. Suc, and C. Gorini (2014), Tectonic inversion of an asymmetric graben: Insights from a combined field and gravity survey in the Sorbas basin, *Tectonics*, 33, doi:10.1002/2013TC003458.

Received 3 OCT 2013

Accepted 9 JUN 2014

Accepted article online 13 JUN 2014

## Tectonic inversion of an asymmetric graben: Insights from a combined field and gravity survey in the Sorbas basin

Damien Do Couto<sup>1,2,3</sup>, Charles Gumiaux<sup>4,5,6</sup>, Romain Augier<sup>4,5,6</sup>, Noémie Le Bret<sup>4,5,6</sup>, Nicolas Folcher<sup>7</sup>, Gwenaél Jouannic<sup>8</sup>, Laurent Jolivet<sup>4,5,6</sup>, Jean-Pierre Suc<sup>2,3</sup>, and Christian Gorini<sup>2,3</sup>

<sup>1</sup>Total S.A. Paris, France, <sup>2</sup>UPMC Université Paris 6, UMR 7193, ISTEP, Paris, France, <sup>3</sup>CNRS, UMR 7193, ISTEP, Paris, France, <sup>4</sup>Université d'Orléans, ISTO, UMR 7327, Orléans, France, <sup>5</sup>CNRS/INSU, ISTO, UMR 7327, Orléans, France, <sup>6</sup>BRGM, ISTO, UMR 7327, Orléans, France, <sup>7</sup>PPME (EA No 3325), Université de la Nouvelle-Calédonie, Nouméa, New Caledonia, <sup>8</sup>CETE de l'Est Laboratoire Régional des Ponts et Chaussées de Nancy, Tomblaine, France

**Abstract** The formation of sedimentary basins in the Alboran domain is associated with the exhumation of metamorphic core complexes over a circa 15 Ma period through a transition from regional late-orogenic extension to compression. An integrated study coupling field analysis and gravity data acquisition was performed in the Sorbas basin in the southeastern Betic Cordillera. Detailed field observations revealed for the first time that extensional tectonics occurred before shortening in this basin. Two extensional events were recorded with NW-SE to N-S and NE-SW kinematics, respectively; the first of which being likely responsible for the basin initiation. Tectonic inversion of the basin then occurred around 8 Ma in an overall approximately N-S shortening context. Two-dimensional gravity sections reveal that the basin acted as an active depocenter as the basin floor locally exceeding 2 km depth is characterized by a marked asymmetric architecture. Based on this integrated study, we explore a new evolutionary scenario which can be used as a basis for interpretations of the Neogene tectonic history of the southeastern Betics.

### 1. Introduction

During the Neogene, the geodynamics of the Mediterranean region was marked by the development of back-arc basins, from the Alboran Sea in the west all the way to the Aegean Sea in the east, initiated after a major change in the subduction regime, during the Oligocene [Rehault *et al.*, 1984; Faccenna *et al.*, 1997; Jolivet and Faccenna, 2000]. The Pannonian Basin, Aegean Sea, Liguro-Provençal Basin, Tyrrhenian Sea and Alboran Sea formed above retreating slabs. The present-day complex geometry of the subduction zones and back-arc basins results from the initial geometry of the African margin [Frizon de Lamotte *et al.*, 2011] and progressive slab tearing and detachments [Wortel and Spakman, 2000] associated with a complex 3D mantle convection pattern [Faccenna and Becker, 2010]. At the western end of the Mediterranean region, the Alboran domain has recorded this regional episode of back-arc extension and slab retreat [Faccenna *et al.*, 2004; Spakman and Wortel, 2004] until ~7–8 Ma before the resumption of a compressional regime due to Africa-Eurasia convergence [Jolivet *et al.*, 2008]. Offshore and onshore sedimentary basins have recorded this evolution and the respective contributions of early extension, and late compression. The final architecture of these basins is still debated, especially in the Huércal-Overa and Sorbas basins [Weijermars *et al.*, 1985; Ott d'Estevou and Montenat, 1990; Augier *et al.*, 2005a; Meijninger and Vissers, 2006; Pedrera *et al.*, 2010]. This study aims at deciphering the respective contribution of extension and subsequent compression in the shaping of the Sorbas basin.

The Sorbas basin, located in the internal zones of the Betic Cordillera (southern Spain), is a key peripheral basin where upper Serravallian to Pliocene sediments have recorded interactions of both tectonic and eustatic changes of the southwestern Mediterranean region. Several scenarios of the Neogene evolution of the whole Alboran region were based upon the stratigraphy and structure of this basin. However, different tectonic settings, from strike slip to pure extension, have been proposed for the initiation of the basin in the Serravallian to lower Tortonian. Since the upper Tortonian, the Sorbas basin has been subjected to NW-SE shortening that has shaped most of its current geometry [Weijermars *et al.*, 1985]. The debate on the tectonic origin of the Sorbas basin is mainly based on contrasting interpretations of the structural relationships between sedimentary basins and metamorphic domes of the adjacent “sierras” (i.e., Sierra de los Filabres and

the Sierra Alhamilla) [Martínez-Martínez and Azañón, 1997; Martínez-Martínez et al., 2002, 2004; Behr and Platt, 2012]. While the Huércal-Overa basin shows rather well-preserved shape and distribution of depocenters linked to the pre-8 Ma extension [Meijninger and Vissers, 2006; Pedrera et al., 2010], late shortening had a major influence on the present-day geometry of the Sorbas basin [Weijermars et al., 1985; Ott d'Estevou and Montenat, 1990]. The effect of the early extension has not yet been discussed, and a better description of the deep structure of the basin is needed to access its early tectonic history. In order to better constrain the geometry of the basin during its evolution, a gravity survey has been carried out through the basin together with new field structural analyses. From these new structural and geometrical constraints, a new tectonic evolutionary scenario is proposed for the Sorbas basin.

## 2. Geological Setting

### 2.1. The Southeastern Betic Cordillera

The Betic Cordillera forms the northern branch of the Betic-Rif orogenic belt that results from the combination of a continental collision between the Alboran domain and the Iberian-Moroccan passive margins, during the Miocene [Crespo-Blanc and Frizon de Lamotte, 2006], and a strong westward movement of the Alboran domain [Lonergan and White, 1997; Faccenna et al., 2004]. The former south Iberian Mesozoic-Cenozoic passive margin currently forms the External Zones of the Betics and corresponds to a fold-and-thrust belt [Platt et al., 2003]. To the South, the finite structure of the Internal Zones results from the stacking of metamorphic units and their subsequent exhumation in the core of metamorphic domes [Martínez-Martínez et al., 2002; Augier et al., 2005a, 2005b]. From bottom to top, the alpine metamorphic basement is composed of the Nevado-Filabride (NF) and the Alpujarride (Alp) complexes, overlain by a third one, the Malaguide (Mal) complex [Torres-Roldán, 1979]. These three complexes are presently separated by crustal-scale extensional shear zones that played a major role during the exhumation of the deeper complexes [García-Dueñas et al., 1992; Lonergan and Platt, 1995; Crespo-Blanc, 1995; Platt et al., 2005; Augier et al., 2005a]. Exhumation of the Alpujarride complex occurred during the early Miocene (22 to 18 Ma) in a N-S to NNE-SSW extensional setting [Monié et al., 1994; Crespo-Blanc et al., 1994; Crespo-Blanc, 1995; Platt et al., 2005]. Timing of peak metamorphic conditions and the inception of exhumation of the NF complex is still debated [López Sánchez-Vizcaino et al., 2001; de Jong, 2003; Augier et al., 2005b; Platt et al., 2006]. Conversely, timing of the final exhumation stages in the greenschists facies conditions spans over the middle and the late Miocene (from 15 to 9 Ma) [de Jong, 1991; Monié and Chopin, 1991; Johnson et al., 1997; Augier et al., 2005b; Platt et al., 2005; Vázquez et al., 2011] through an ~E-W regional-scale extension [Jabaloy et al., 1992]. Final exhumation stages in the brittle regime at circa 13–12 Ma were accompanied by the development of extensional sedimentary basins such as the Huércal-Overa basin [Vissers et al., 1995; Augier, 2004; Meijninger and Vissers, 2006; Augier et al., 2013].

The Sorbas basin belongs to a mosaic of E-W oriented late Neogene intramontane basins with the Huércal-Overa basin and the Almanzora Corridor, to the North, the Alpujarran Corridor to the West, and the Vera basin to the East [Ott d'Estevou and Montenat, 1990; Sanz de Galdeano and Vera, 1992; Iribarren et al., 2009; Pedrera et al., 2010]. It is bounded to the North by the Sierra de los Filabres and to the South by the Sierra Alhamilla (Figure 1), two E-W elongated metamorphic domes [Platt and Vissers, 1989; Vissers et al., 1995; Martínez-Martínez and Azañón, 1997] formed by the exhumation of the NF complex and amplified by later folding [Weijermars et al., 1985].

### 2.2. Tectonic and Geodynamic Framework

The extensional regime which affected the Betic Cordillera and, in a more regional extent, the entire Alboran domain started from the late Oligocene to early Miocene (see Vergés and Fernández [2012] for a review of tectonic evolution) and is widely documented both offshore [Watts et al., 1993; Comas et al., 1999] or onshore [García-Dueñas et al., 1992; Galindo-Zaldívar et al., 2003], especially in the Huércal-Overa basin [Briand et al., 1990; Augier et al., 2005a; Meijninger and Vissers, 2006; Pedrera et al., 2009, 2010, 2012; Augier et al., 2013]. This later displays an overall half-graben geometry accompanied by mesoscale to small-scale synsedimentary normal faults. Its formation and its development have been associated with the exhumation of the NF metamorphic complex in the Sierra de Los Filabres metamorphic dome [Augier et al., 2005a; Meijninger and Vissers, 2006; Augier et al., 2013] (see Figure 1). According to Augier et al. [2013], the half-graben geometry results from the development of north dipping normal faults that are probably rooted in the detachment

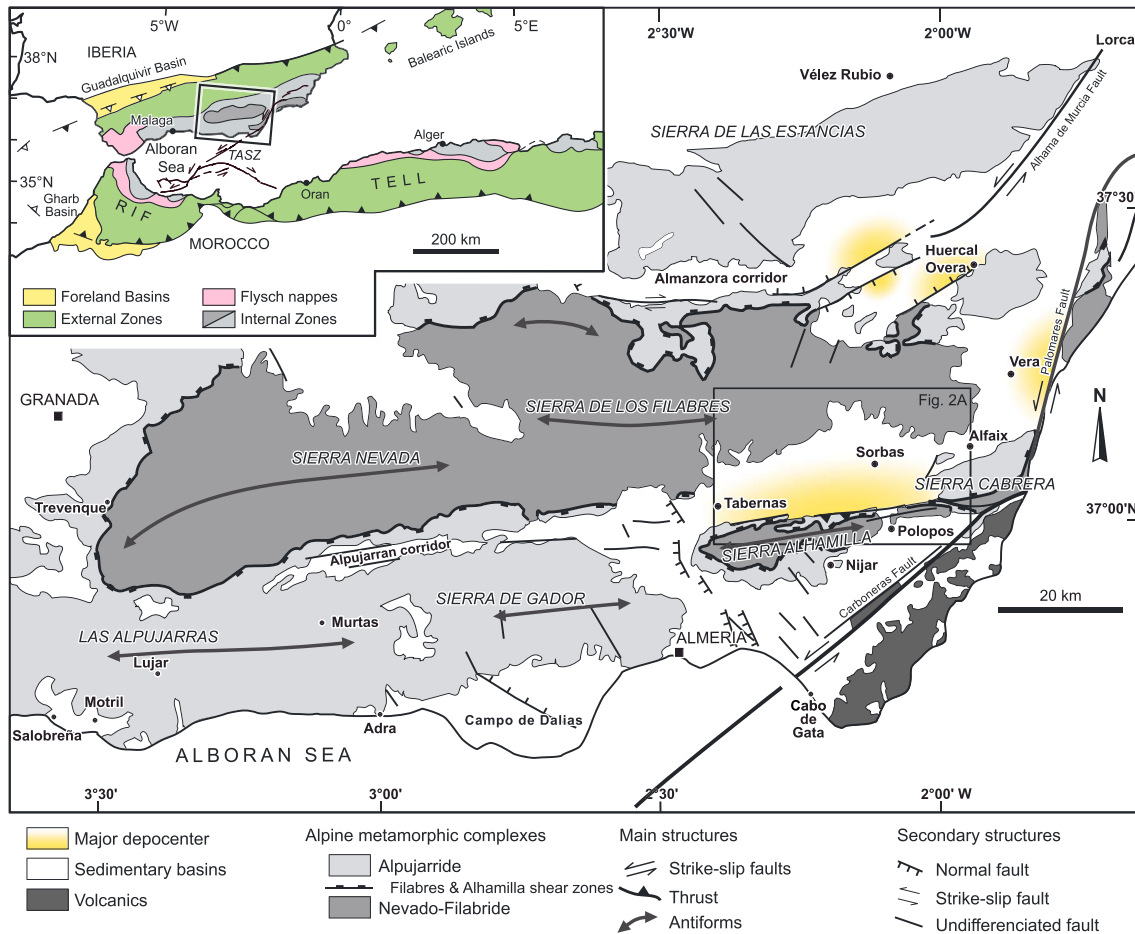


**Figure 1.** Simplified structural map of southeastern Spain. Located are the main metamorphic domes of the Sierra de los Filabres/Neveda and the Sierra Alhamilla/Cabrera and the main sedimentary basins modified after Augier *et al.* [2005b]. Also indicated are the main tectonic contacts such as the Filabres and Alhamilla shear zones and the prominent sinistral fault zones pertaining to the Trans-Alboran transcurrent zone (CF: Carboneras Fault, PF: Palomares Fault, and AMF: Alhama de Murcia Fault) and smaller-scale structures.

separating the NF from the Alp complexes, called the Filabres Shear Zone. A similar tectonic contact (called the Alhamilla detachment [García-Dueñas *et al.*, 1992; Martínez-Martínez and Azañón, 1997]) also crops out in the Sierra Alhamilla. Last motions on that detachment in ductile conditions occurred at circa 14–13 Ma [Martínez-Martínez and Azañón, 1997; Augier *et al.*, 2005b; Platt *et al.*, 2005], while exhumation tectonics under the brittle regime lasted until circa 8 Ma.

Unlike the Huércal-Overa basin, the Sorbas basin presents evidences for compression tectonics (Figure 2). The northern boundary of the basin is characterized by an overall gentle onlap of the sediments over the basement of the Sierra de Los Filabres (Figure 2b). Conversely, in the southern part of the basin, Tortonian sediments are folded, locally overturned or even overthrust by basement rocks (Figure 3) [Weijermars *et al.*, 1985; Ott d'Estevou and Montenat, 1990; Giaconia *et al.*, 2012a, 2013]. The onset of compression in the region has been ascribed to the upper Tortonian at around 8 Ma [Weijermars *et al.*, 1985; Comas *et al.*, 1999; Augier, 2004; Jolivet *et al.*, 2006; Meijninger and Vissers, 2006; Augier *et al.*, 2013]. This compressional regime resulted in the formation of the current E-W oriented open-fold syncline geometry of the Messinian to Quaternary series [Weijermars *et al.*, 1985; Ott d'Estevou and Montenat, 1990] (Figure 2b).

Based on field investigations, several hypotheses were proposed to explain the initiation phase of both the Sorbas [Montenat *et al.*, 1987; Weijermars *et al.*, 1985; Ott d'Estevou *et al.*, 1990; Poisson *et al.*, 1999] and Tabernas basins [Kleverlaan, 1989]. These mainly differ on the interpretation of the regional-scale tectonic regime occurring at that time:

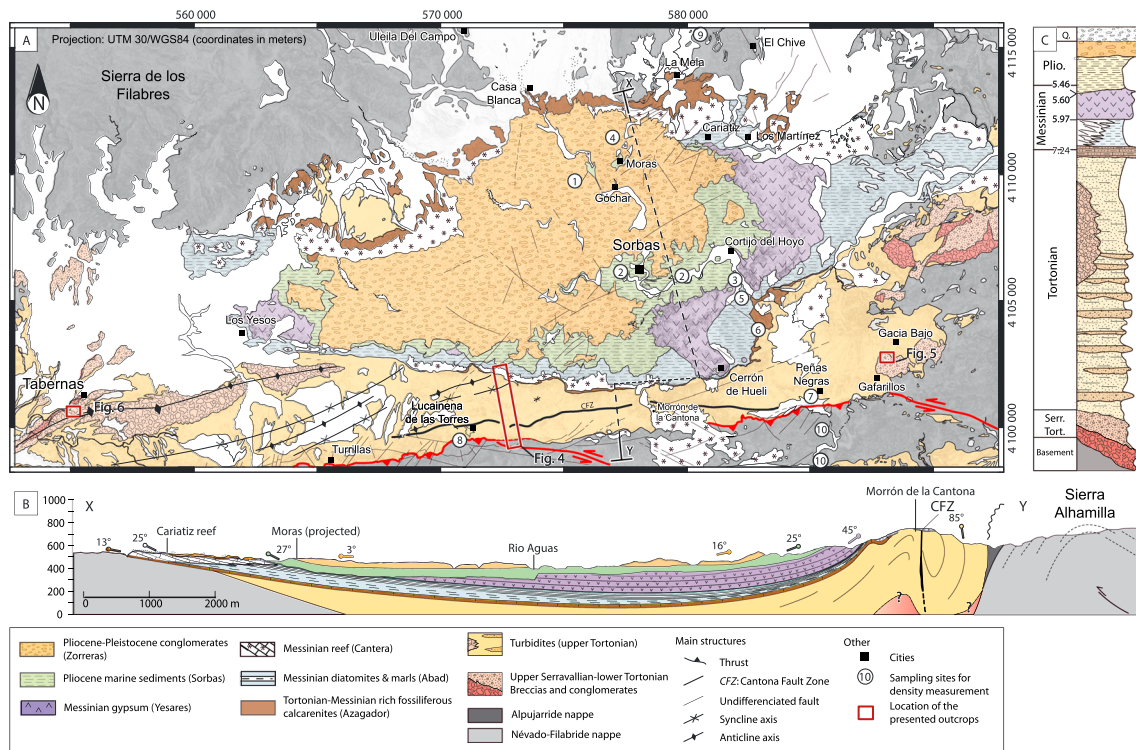


**Figure 2.** Structure and stratigraphy of the Sorbas basin. (a) Geological map of the Sorbas basin, modified from Ott d'Estevo and Montenat [1990] and García Monzón et al. [1974]. Projection UTM Zone 30 (WGS84 ellipsoid). (b) Synthetic N-S cross-section X-Y representing the main architecture of the Sorbas basin (location in Figure 2a). (c) Synthetic stratigraphic log of the Sorbas basin. Modified after Montenat and Ott d'Estevo [1977], Ott d'Estevo and Montenat [1990], Krijgsman et al. [1999], Krijgsman et al. [2001], and Manzi et al. [2013].

1. Compressional to transpressional models with an overall N-S oriented maximum shortening have been put forward [Montenat et al., 1987; Weijermars et al., 1985; Ott d'Estevo et al., 1990; Sanz de Galdeano and Vera, 1992; Poisson et al., 1999]. They all consider the Africa/Europe convergence as the principal driving force controlling crust deformation [Sanz de Galdeano, 1985; Ott d'Estevo and Montenat, 1990]. In these models, the Sorbas basin is interpreted either (i) as a purely flexural basin developed along a major EW trending/northward verging thrust [Weijermars et al., 1985] or (ii) a transpressional basin linked to a wide NE-SW strike-slip shear zone [Sanz de Galdeano, 1985; Weijermars, 1987; Montenat et al., 1987; Ott d'Estevo and Montenat, 1990; Sanz de Galdeano and Vera, 1992; Stapel et al., 1996].
2. A strike-slip fault network is active since the middle/upper Miocene [Sanz de Galdeano, 1985; Booth-Rea et al., 2004a; Sanz de Galdeano et al., 2010; Rutter et al., 2012] and corresponds to the onshore extension of the Trans-Alboran shear zone (Figure 1) [de Larouzière et al., 1988]. In that context, the deposition of Tortonian sediments would have taken place in a pull-apart trough [Kleverlaan, 1989; Stapel et al., 1996; Haughton, 2001; Martínez-Martínez et al., 2006; Rutter et al., 2012].
3. Extensional models in which the formation of asymmetric intramontane basins are linked to the late exhumation stages within the metamorphic domes of the NF metamorphic complex during the collapse of the Internal Zones [García-Dueñas et al., 1992; Vissers et al., 1995; Martínez-Martínez and Azañón, 1997; Meijninger and Vissers, 2006; Augier et al., 2013]. Basins would be initially extensional during the upper Serravallian to lower Tortonian [Meijninger and Vissers, 2006; Augier et al., 2013] before they experience inversion tectonics from upper Tortonian to Quaternary.

Recent gravity surveys show an irregular and/or asymmetrical distribution of the residual gravity anomalies in the Almanzora Corridor (Figure 1) [Pedrera et al., 2009], in the Sorbas basin [Li et al., 2012] and in the Huércal-Overa basin [Pedrera et al., 2010]. The Huércal-Overa area has been particularly well documented: modeled gravity profiles evidence that the deepest parts of the sediment/basement interface, reaching 1000 to 1500 m depth, are confined to the southern part of the basin [Pedrera et al., 2009, 2010] and more particularly along normal faults [Augier et al., 2013]. Besides, tectono-stratigraphic and paleostress analyses from brittle fault show that two main

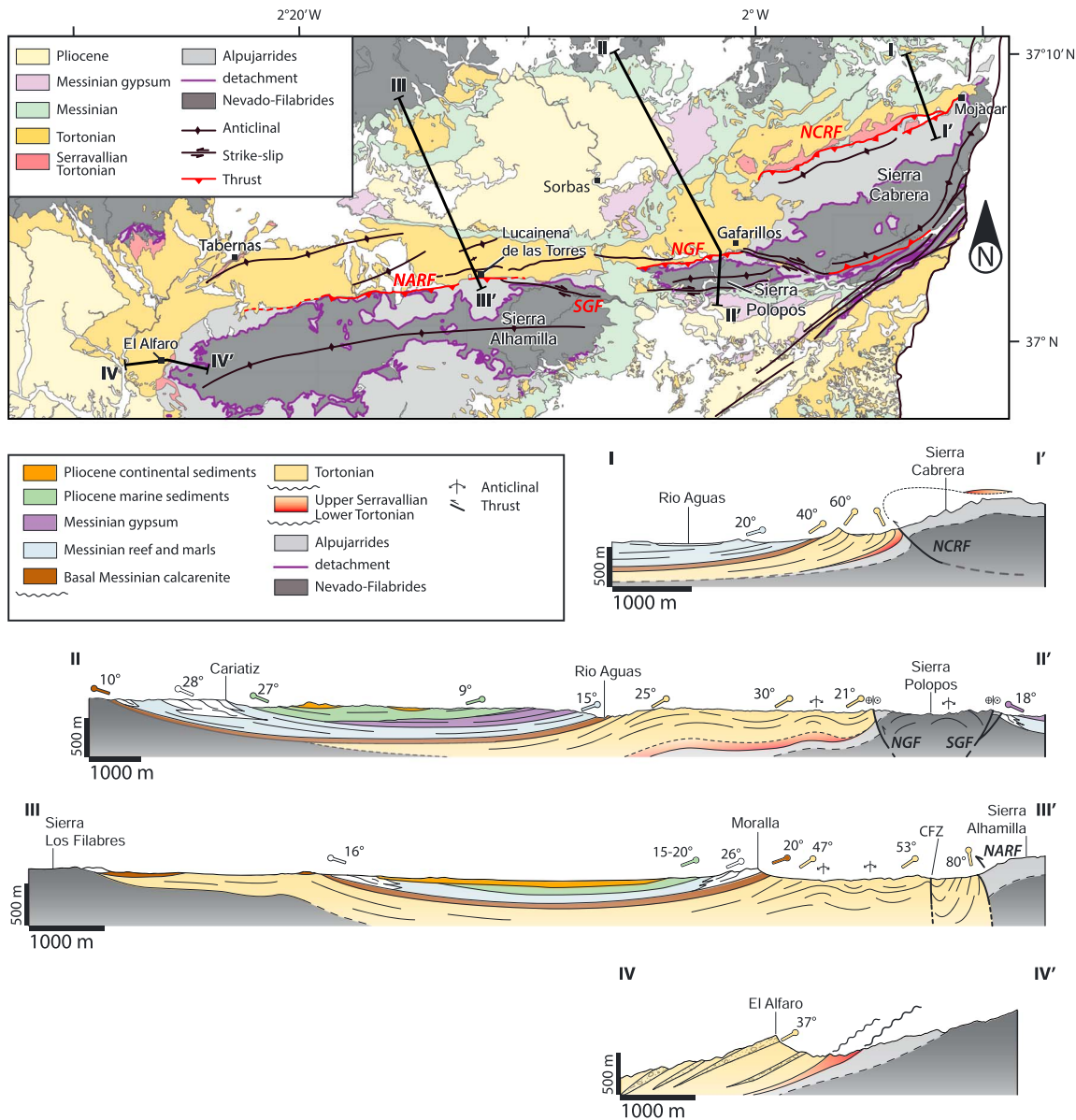


**Figure 3.** Simplified geological map showing the four main faults accommodating the deformation along the Sierra Alhamilla, Sierra Polopos, and Sierra Cabrera: from East to West, the North Cabrera reverse fault (NCRF), the North Gafarillos fault (NGF), the South Gafarillos Fault (SGF), and the North Alhamilla reverse fault (NARF). Four cross sections, orthogonal to the sediments/basement contact, present the geometry and architecture of the sedimentary units with respect to the metamorphic ridges (location of cross sections in the geological map). See text for more details.

depocenters were first controlled by SW-NE trending normal faults probably rooting in the Filabres Shear Zone [Augier *et al.*, 2013]. This brittle extensional event occurred during the latest Serravallian to lower Tortonian (~12–11 Ma) and is linked to the exhumation of the NF metamorphic complex [Augier *et al.*, 2013]. Sedimentation started during the late denudation stages of the NF complex as evidenced by zircon and apatite fission track ages and U-Th/He analyses on apatites (respectively at  $11.9 \pm 0.9$  Ma,  $8.9 \pm 2.9$  Ma, and  $8.7 \pm 0.7$  Ma) [Johnson *et al.*, 1997; Vázquez *et al.*, 2011] in both the Sierra de los Filabres and Alhamilla [Augier *et al.*, 2005b; Platt *et al.*, 2005].

### 3. The Sorbas Basin

#### 3.1. Basement Units Bounding the Basin

While the Malaguide complex is poorly represented within the study area, the Alpujarride and the Nevado-Filabride complexes are both well exposed within the metamorphic domes forming the sierras [Vissers *et al.*, 1995;

*Martínez-Martínez and Azañón, 1997*). The Alpujarride complex is mostly represented by Permian purple to reddish phyllites overlain by Triassic metacarbonates [*García Monzón et al., 1973b, 1974; Azañón and Crespo-Blanc, 2000*]. The Nevado-Filabride complex is made of three main units [*García-Dueñas et al., 1988; de Jong, 1991*] called, from bottom to top, the Ragua Unit, the Calar-Alto Unit, and the Bédar-Macael Unit with respective average structural thicknesses of about 4000, 4500, and 600 m [*Martínez-Martínez et al., 2002*]. The Ragua Unit is made up of Paleozoic dark micaschists with intercalated quartzites and rare dark marbles [*Martínez-Martínez, 1985*], while the Calar-Alto and the Bédar-Macael units mainly contain Paleozoic black micaschists, Permo-Triassic quartzites, metapelites, and Triassic metacarbonates. Dense eclogite and blueschist bodies or their retrogressed equivalent amphibolite-facies metamorphic rocks are described as metric to kilometeric scattered lenses into both Calar-Alto and Bédar-Macael units [*García Monzón and Kampschuur, 1972; García Monzón et al., 1973a; Martínez-Martínez and Azañón, 1997*].

### 3.2. Stratigraphy

The oldest sedimentary record of the Sorbas basin surroundings is represented by scarce Burdigalian-Langhian marly limestones badly preserved north to the Sierra Cabrera and Serravallian shallowing upward turbidites exposed along the Sierra Alhamilla and Sierra Cabrera (Figure 1) [*Ott d'Estevou and Montenat, 1990; Sanz de Galdeano and Vera, 1992*]. The rest of the series is quite similar to nearby basins [*Sanz de Galdeano and Vera, 1992*] and starts with two different units [*Ott d'Estevou and Montenat, 1990*]: (i) a ~100 m thick upper Serravallian to lower Tortonian continental coarse-grained deposits evolving basinward to yellowish marls and turbidites (Figure 2c), which outcrop in the western (i.e., Tabernas area) and eastern (i.e., Gafarillos area) parts of the basin (Figure 3a) and (ii) a rather thick (up to 2000 m according to *Ott d'Estevou and Montenat [1990]*) upper Tortonian marine unit, composed of grayish to yellowish sandstones and turbidites (Figure 2c). It is worth mentioning that deposition of the upper Serravallian to lower Tortonian sediments appear coeval with the latest exhumation of the NF complex in the surrounding sierras [*Ott d'Estevou and Montenat, 1990; Johnson et al., 1997; Vázquez et al., 2011*]. Latest Miocene sediments unconformably overly Tortonian sediments and are composed of six units including from bottom to top (Figure 2c): (a) a shallow-marine fossiliferous calcarenite (Azagador member) dated from the Tortonian/Messinian boundary [*Ott d'Estevou and Montenat, 1990; Sierro et al., 1993; Krijgsman et al., 2001*]; its thickness ranges from 10 to 80–90 m depending on its paleogeographical context [*Ott d'Estevou and Montenat, 1990; Puga-Bernabéu et al., 2007*]; (b) an early Messinian marly unit known as the Abad marls composed of ~120 m of marls alternating with diatomites. The upper part passes laterally to plurimetric fringing reefal carbonates (Cantera member; Figure 2) outcropping both in the northern and in the southern part of the basin (e.g., Cariatiz and Morrón de la Cantona localities; Figure 2a), bounding the basin during the early Messinian [*Martín et al., 1999*]; (c) a 120 m thick evaporitic unit (Yesares member) consisting in gypsum alternating with clayey to marly laminites [*Dronkert, 1976*] deposited during the Messinian Salinity Crisis [*Clauzon et al., 1996; CIESM, 2008*] whose onset is calibrated at 5.971 Ma [*Manzi et al., 2013*]; (d) a latest Messinian to early Pliocene lagoonal calcarenite (Sorbas member) [*Roep et al., 1998*] passing to a Gilbert-type fan delta (dated from 5.46 to 5.00 Ma); the thickness of this marine unit reaches 75 m in the center of the basin at Sorbas locality; and (e) finally, a mostly continental sedimentary unit made of reddish conglomerates called the Zorreras member and reaching 60 m in the basin [*Montenat et al., 1980; Martín-Suárez et al., 2000*].

## 4. Aims and Approach

Most of the studies on the Sorbas basin, having poor structural claims, focused on the Messinian history [*Rouchy and Saint-Martin, 1992; Clauzon et al., 1996; Roep et al., 1998; Riding et al., 1998, 2000; Martín et al., 1999; Krijgsman et al., 2001; Braga et al., 2006; Bourillot et al., 2009; Roveri et al., 2009*]. Besides, while the overall structure of the post-Tortonian deposits is documented as the consequence of a ~N-S compressional context (see above), the tectonic control during the onset of subsidence and early development of the basin remains debated and in fact mostly unexplored. This study aims at constraining the kinematics of the Sorbas basin while the basin underwent its first subsidence phase and sedimentary deposition during the upper Serravallian to lower Tortonian. This paper thus focuses not only on the structure of the early deposits/basement contact which outcrops along the southern margin of the basin but also on the 3-D geometry of this contact, to depth. It also deals with the kinematics and stress conditions that prevailed during the upper Serravallian to lower Tortonian period. Geological and geophysical data have been used and integrated in this work including structural geology, mapping, paleostress computations, and gravimetric survey and modeling.

At first, a synthesis on the structure of the southern margin of the basin (i.e., the northern edge of the metamorphic Sierras) is made with a particular focus on the contact between Serravallian-Tortonian sedimentary units and the basement. It is based on a compilation of existing data and own field observations. Then, structural and kinematical constraints are given from structural field observations made in the older deposits of the basin, in specific areas. As shown before, earliest deposits of the upper Serravallian to lower Tortonian are poorly exposed in the study area because of the extension of post-Tortonian sedimentary series (Figures 2c and 3a) and the ongoing deformation. However, systematic and accurate structural measurements have been realized along the southern basin margin where outcropping conditions allow observing various kinematic constraints. To first describe the initial development of the Sorbas basin and to insure an accurate determination of the deformation kinematics, paleostress orientation patterns were evaluated by the computer-aided inversion method of fault-slip data [Angelier, 1984, 1990]. Thanks to the recognition of numerous stratigraphic time markers including major unconformities [Ott d'Estevou and Montenat, 1990; Sanz de Galdeano and Vera, 1992], the succession of stress regimes is reasonably well constrained in time. As detailed in the following (see *Structural Analysis*), the study focused on (i) the structure of the basement/sedimentary rocks interface, (ii) structural analyses and inversion of fault-slip data to obtain paleostress tensors carried out in the Serravallian-Tortonian series, and (iii) of their internal structures.

Gravity data modeling has already proven its efficiency for imaging deep geological structures at crustal scale, especially for "basement" rock-type imaging in plutonic and metamorphic geological environments [Rousset et al., 1993; Lefort and Agarwal, 1999; Martelet, 1999; Martelet et al., 2004; Talbot et al., 2004; Joly et al., 2009; Turrillot et al., 2011]. While gravity modeling is more rarely applied to sedimentary geological environments [Szafián and Horváth, 2006; Pedrera et al., 2009, 2010; Li et al., 2012; Salcher et al., 2012], this method is used here, in particular, to constrain the geometry of the interface between the rather dense basement rocks of the metamorphic complexes and the lighter sediments of the basin. Deep structures of the basin are thus constrained along a series of 2-D gravity profiles overlapping the basin and the surrounding basement units. Gravity models and field observations, including bedding orientation measurement, were finally used to interpolate the 3-D basin floor geometry. These results allow improving our knowledge on the tectonic evolution during the development of the Sorbas basin and precisising the structural control on deposits geometry.

## 5. Structural Analysis

### 5.1. Evidence of Compressive Tectonics

The Sierra Alhamilla, Sierra Polopos, and Sierra Cabrera represent three E-W elongated en echelon antiforms (Figure 3). The Alhamilla and Polopos ranges form two north verging asymmetric folds with a north steep-dipping forelimb and a gentle south dipping backlimb [Platt et al., 1983]. They are together separated from the Sierra Cabrera by the dextral North Gafarillos strike-slip fault (NGF, Figure 3). The northern front of the Sierra Alhamilla, Polopos, and Cabrera antiformal structures are composed of three major faults called, from East to West, the North Cabrera reverse fault (NCRF), the North Gafarillos fault (NGF) and the North Alhamilla reverse fault (NARF) [Giaconia et al., 2012a, 2012b, 2013] (Figure 3).

The North Cabrera reverse fault affects the entire sedimentary filling and shows inverted or strongly dipping Serravallian and Tortonian sediments with a N to NW transport striking [Booth-Rea et al., 2004b] (cross-section I-I', Figure 3). According to Booth-Rea et al. [2004b], the activity of the NCRF initiated before the upper Tortonian as upper Tortonian conglomerates unconformably overlies Langhian-Serravallian deposits. The fault activity is related to the initiation of major sinistral Palomares and Carboneras strike-slip faults [Booth-Rea et al., 2004b; Gracia et al., 2006; Giaconia et al., 2012a]. The North Gafarillos and South Gafarillos faults (NGF and SGF, Figure 3) represent two transpressive dextral faults accommodating the deformation and the relative displacement of the Sierra Alhamilla with the Sierra Cabrera [Giaconia et al., 2012a]. The E-W segment of the NGF, bounding the Sorbas basin to the south, affects the Tortonian series (cross-section II-II' in Figure 3), and most of the deformation occurred during the Tortonian as Messinian reefal carbonates seal the contact toward the West (Cantera Member, Figures 2b and 3) [Ott d'Estevou and Montenat, 1990; Stapel et al., 1996; Jonk and Biermann, 2002]. The E-W North Alhamilla reverse fault zone, which is linked to the South Gafarillos dextral strike-slip fault, can be followed over ~20 km along the southern border of the Sorbas-Tabernas basin. This thrust fault zone cuts the northern limb of the asymmetric Alhamilla antiform where Serravallian-Tortonian deposits display overturned bedding just below (Figure 2; cross-section III-III' in Figure 3). Its activity lasted from

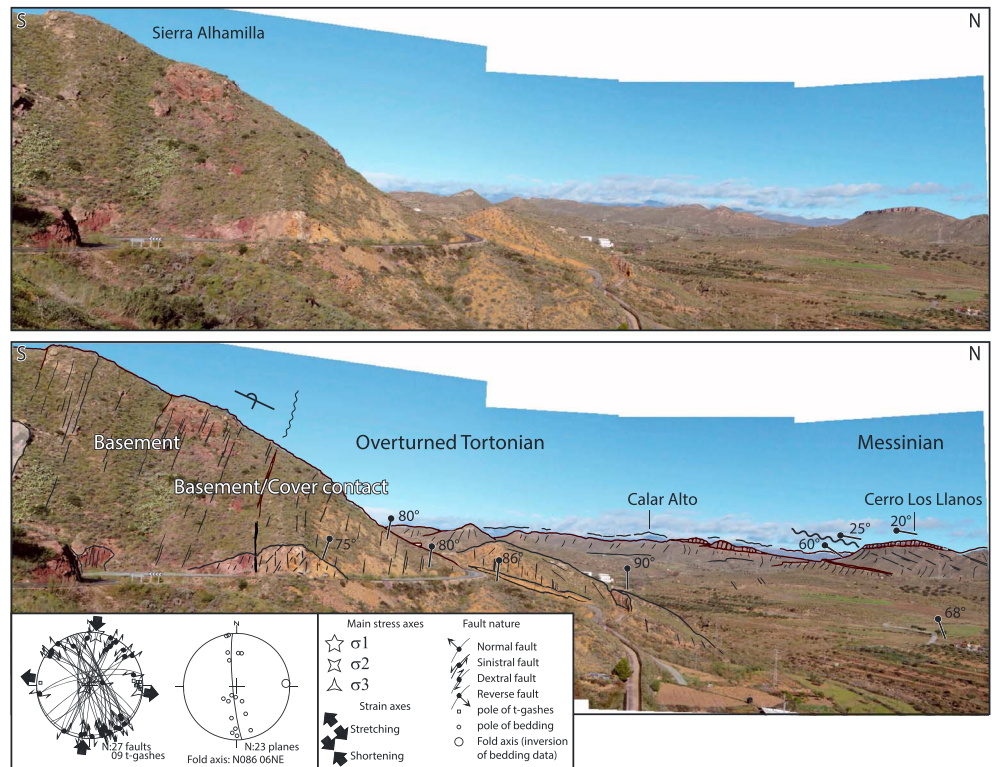


**Figure 4.** Evidences of upper Tortonian compressive tectonic. Panoramic view of the southern folded boundary of the Sorbas basin East of Lucainena de las Torres (see location in Figure 2). Here the metamorphic basement describes a north verging asymmetric fold with an overturned steep-dipping forelimb. Tortonian series, separated from the basement by an unconformity, display a rather continuous growth-strata structure forming a recumbent syncline. Fault-slip data inversion indicates a N-S maximum compression direction [ $\sigma_1$ ].

the upper Tortonian to the late Pleistocene with an overall top-to-the-NNW movement and controls the front of the Sierra Alhamilla range by a drastic topographic gradient [Jonk and Biermann, 2002; Giaconia et al., 2012a]. Several studies pointed out the syncompression filling of upper Tortonian series [Weijermars et al., 1985; Ott d'Estevou and Montenat, 1990; Haughton, 2001], reporting a southward progressive gradient of deformation. Toward the west of the Sierra Alhamilla, the NARF disappears, and the nature of the contact separating Serravallian-Tortonian deposits from the Alpujarrides metamorphic series appears unconformable (cross-section IV-IV' in Figure 3). There, the El Alfaro hill which is made of plurimetric conglomeratic and sandy interval belongs to the upper Tortonian turbiditic series [Hodgson and Haughton, 2004]. According to Haughton [2000] and Hodgson and Haughton [2004], the timing of deformation in the Alfaro area is also estimated as Tortonian and Messinian in age from the sedimentary record (thick slump deposits and internal unconformities).

The overthrust of the Sierra Alhamilla basement range over the southern border of the basin marks the strong asymmetry of both the basin and the basement range [Ott d'Estevou et al., 1990; Martínez-Martínez and Azañón, 1997]. The NARF disappears toward the East of Lucainena de las Torres (Figure 3), Figure 4 displays a landscape interpretation accompanied with bedding measurements made across the basement/sediments contact (see Figure 2 for location). The bedding attitude of the Tortonian series shows a progressive steepening over more than 2 km and is even overturned in the vicinity of the Sierra Alhamilla (Figure 4), fold asymmetry being illustrated by the more pronounced clustering of bedding poles in stereonet projection (Figure 4). Structurally below, to the south, metasediments of the basement units show parallel overturned bedding orientation to the basal layers of the basin marking an overturned forelimb of the Sierra Alhamilla. There, upper Tortonian sediments are separated from the basement by an unconformity or a stratigraphic break as the upper Serravallian to lower Tortonian continental series are missing. East of the NARF, the geometry of the basement/sediment interface argues in favor of a north verging asymmetric fold in the Sierra Alhamilla with an overturned steep-dipping forelimb, highlighting the recumbent syncline of Tortonian deposits. Such folded structure could be interpreted as a fault-propagation fold.

Progressive unconformities (e.g., growth-strata) in upper Tortonian sediments (8–7.24 Ma) mark the growth of the Sierra Alhamilla basement range and determine a good age control on that deformation episode. This compressional episode mostly shaped the current geologic and topographic features of the southeastern parts of the Internal Zones of the Betic Cordillera and predates the Messinian to the present evolution of the basin. Indeed, the overlying Messinian carbonates seal most of the folding linked with the growth of the Sierra Alhamilla range (Figures 2 and 3) [Weijermars *et al.*, 1985; Ott *d'Estevou and Montenat*, 1990] but are in turn involved in the present-day large-scale open fold of the Sorbas basin. Internal deformation of the upper Tortonian series is characterized by small-scale wrench faulting with only rare reverse faults as shown along the road-cut near Lucainena de las Torres (Figure 4). Analysis of fault-slip data yielded a strike-slip paleostress tensor solution with a N-S maximum compression direction [ $\sigma_1$ ] and a W-E minimum compression direction [ $\sigma_3$ ] in that case, consistent with the large-scale folding of the northern front of the Sierra Alhamilla (Figures 2b and 4).

## 5.2. Evidence of Extensional Deformation

Upper Serravallian to lower Tortonian deposits, which are particularly abundant in the Huércal-Overa basin, are in contrast very limited within the Tabernas-Sorbas basins. They are encountered along the northern limb of Sierra Alhamilla (Figure 3). These deposits are of prime importance with respect to the deep structure of the basin and consequently with the buried history of the Sorbas basin. Hereafter, two groups of outcrops are described as representative of that discussion, the Tabernas and the Gafarillos areas (see location in Figure 2).

In the Gafarillos area, upper Serravallian to lower Tortonian formations crop-out well along roads that cross the hills, particularly the approximately N020E striking road linking Gafarillos to Gacia-Bajo. There, the sedimentation, characterized by conglomerates and coarse-grained sandstones, presents general subhorizontal bedding and is affected by a pervasive network of small-scale normal faults (Figure 5a) locally showing synsedimentary character (Figure 5b). The entire normal faults population, generally developed as 50–70° dipping roughly planar surfaces, presents two distinctive orientations: a dominant approximately N140E and a subordinate approximately N030E conjugate sets of normal faults. Associated stress tensors correspond to subhorizontal extension presenting respectively N060E and N140E minimum compression direction [ $\sigma_3$ ] and a common subvertical maximum compression direction [ $\sigma_1$ ] (Figure 5a). Analysis of younger rocks belonging to the basal upper Tortonian in the same area (Figure 5c, inset), revealed that only the approximately N140E set of normal faults was present, suggesting that the former N30E system was restricted to the upper Serravallian to lower Tortonian formations.

The Tabernas area provides an example of geometrical relationships between faulting and folding (see location on Figure 2). There, upper Serravallian to upper Tortonian formations experienced a large-scale folding episode (i.e., the so-called Tabernas fold) [Ott *d'Estevou and Montenat*, 1990] particularly well exposed along the incised Rambla de la Sierra. A landscape picture is given on Figure 6. In details, the whole area presents a pervasive network of small-scale faults systems including mostly normal and wrench faults whose relative chronology and relationships with folding remained so far unexplored. Close-up views of two parts of the northern limb of the fold are given as insets in Figure 6; inset B documents faulting in the upper Serravallian to lower Tortonian formations and inset C, the upper Tortonian. Moreover, Figure 6d provides a decomposition of the total heterogeneous fault population into homogeneous, cogenetic fault populations. Normal faulting appears clearly related to prefolding extension as suggested by the coexistence of both subvertical and subhorizontal normal and reverse faults (in the present attitude of bedding) passively rotated with respect to bedding (Figures 6b and 6c). In addition, it is to be noted that some of them reveal a synsedimentary character. Computed principal stress regimes, in agreement with an Andersonian model after back tilting [Anderson, 1942], yielded a succession of two subhorizontal extensional regimes with N50E and N140E minimum compression direction [ $\sigma_3$ ] for an almost vertical common maximum compression direction [ $\sigma_1$ ]. Wrench faults that often reactivate former normal fault planes present N20–80E sinistral faults accompanied by N120–170E dextral faults. Analysis of fault-slip data yielded a strike-slip paleostress tensor solution characterized by a N-S maximum compression direction [ $\sigma_1$ ] and a W-E minimum compression direction [ $\sigma_3$ ]. This result is consistent with the large-scale W-E folding that affect passively the Sierras [Weijermars *et al.*, 1985; Ott *d'Estevou and Montenat*, 1990] and the basins (Figures 2 and 3) with an approximately 10–20° dispersion as exemplified by the WSW-ENE Tabernas anticline (Figure 6d).

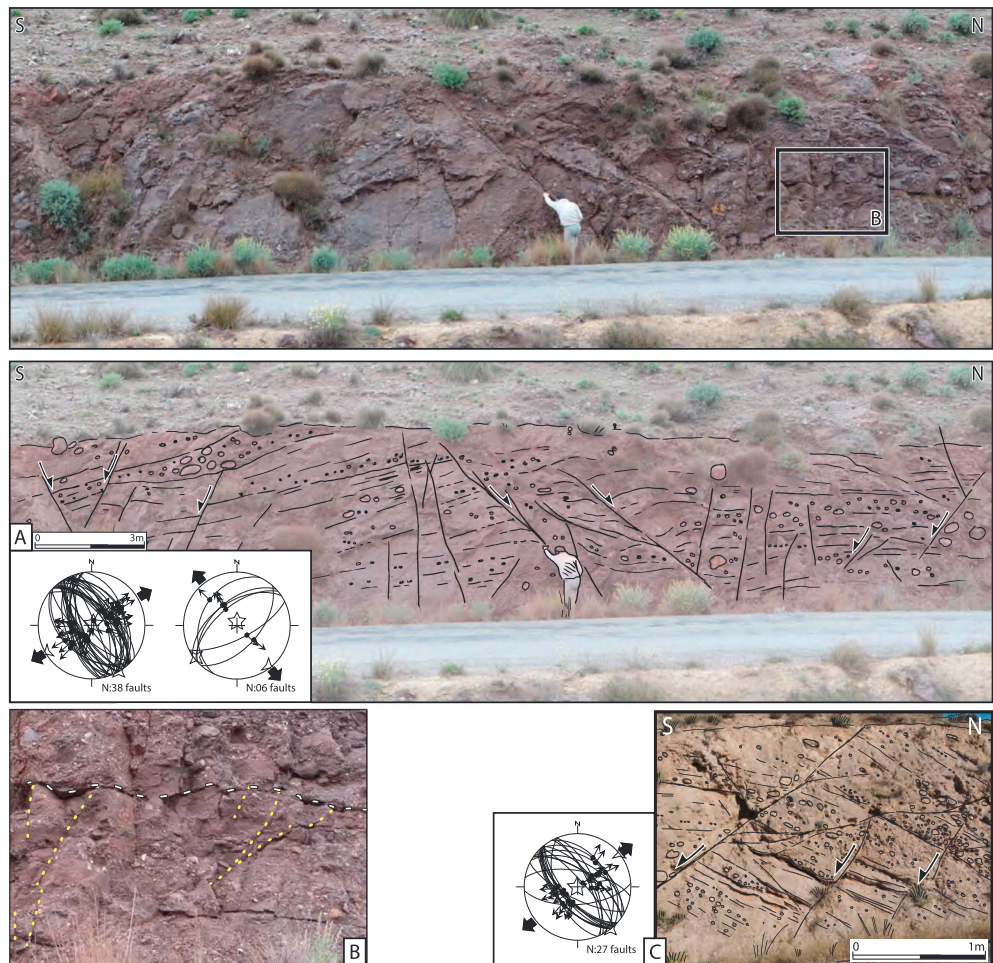


**Figure 5.** Field evidences of extensional deformation affecting upper Serravallian to upper Tortonian sediments, (location in Figure 2). (a) Uninterpreted and interpreted panorama of lower Tortonian reddish conglomerates affected by two sets of small-scale normal faults: a dominant approximately N140E and a subordinate approximately N30E conjugate sets of normal faults. (b) A close-up view of syndepositional normal faults affecting sandy to microconglomerate intervals and interrupted by a coarse-grained conglomerate. (c) Upper Tortonian marine sediments affected by a N140E oriented set of small-scale normal faults.

The structural development and the sedimentation of the Tabernas-Sorbas basin thus appear controlled by normal faulting from upper Serravallian to lower Tortonian onward and at least during a part of the upper Tortonian. These traces of extension whose origin appear coeval and may be related with the regional-scale exhumation of the Nevado-Filabride metamorphic complex [Martínez-Martínez and Azañón, 1997; Augier et al., 2005a, 2013] are now mostly hidden by thick younger deposits in the Sorbas basin area.

## 6. Two-Dimensional Gravity Survey

### 6.1. Acquisition and Treatment

A gravity survey was conducted throughout the Sorbas basin and surrounding basement areas. Ground measurements were performed using a SCINTREX CG5-M microgravimeter in 195 gravity stations emplaced along 6 ~ north-south trending sections, orthogonal to regional-scale structures, and one additional longitudinal (i.e., ~east-west) section for crosschecking (Figure 7). Measurement stations were spaced approximately 1 km apart along the two longer sections aiming at imaging regional-scale structures (see N-S trending SCS1 “Sorbas Cross-Section 1” and SCS2 E-W trending section; Figure 7). Along other profiles, stations were spaced approximately 500 m apart within the Sorbas basin and approximately 250 m apart along the segments in the vicinity of the basement/sediment contact. To better control the raw data quality, measurements were

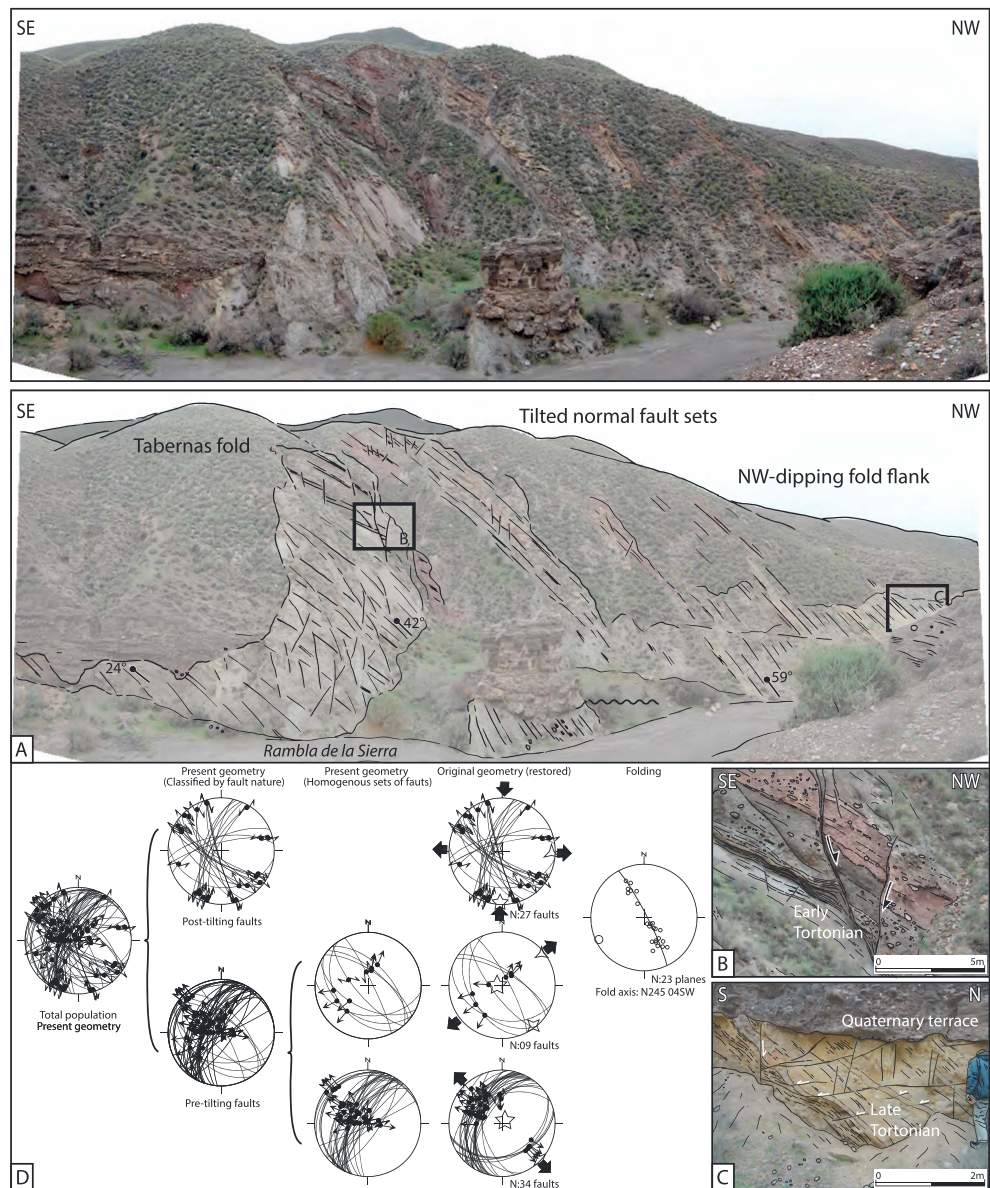


**Figure 6.** Geometrical relationships existing between the upper Serravallian-Tortonian extensional deformation and the upper Tortonian inversion. (a) Uninterpreted and interpreted panoramic view of the northern flank of the so-called Tabernas fold [Ott d'Estevou and Montenat, 1990] showing (b) the presence of tilted normal faults affecting the lower Tortonian deposits and also (c) the upper Tortonian marine sediments. (d) The decomposition of the total heterogeneous fault population into homogeneous, cogenetic fault populations shows the presence of two subhorizontal extensional regimes with N50E and N140E minimum compression direction ( $\sigma_3$ ) that predate inversion tectonics visible at all scales from microfaults to large-scale folding.

repeated 3 times at each gravity station. Geographic coordinates and altitude were measured using a MAGELLAN Promark3 post-D-GPS system. For each station, location was recorded and averaged during more than 1 min, and values were adjusted through a posttreatment correction process by using a secondary antenna that was fixed for the entire survey period. Such acquisition method ensures approximately 10 cm and 20 cm of precision for horizontal and vertical coordinate values, respectively. To ensure consistency between the different gravity profiles measured and to control the temporal instrumental drift, a unique gravity reference station was used during the overall field survey; it was systematically measured twice a day, before and after daily surveys (Figure 7b, Los Martinez locality). To calculate the Bouguer anomaly, standard free air, plateau, and terrain corrections were successively performed; a  $2.67 \text{ g cm}^{-3}$  Bouguer reduction

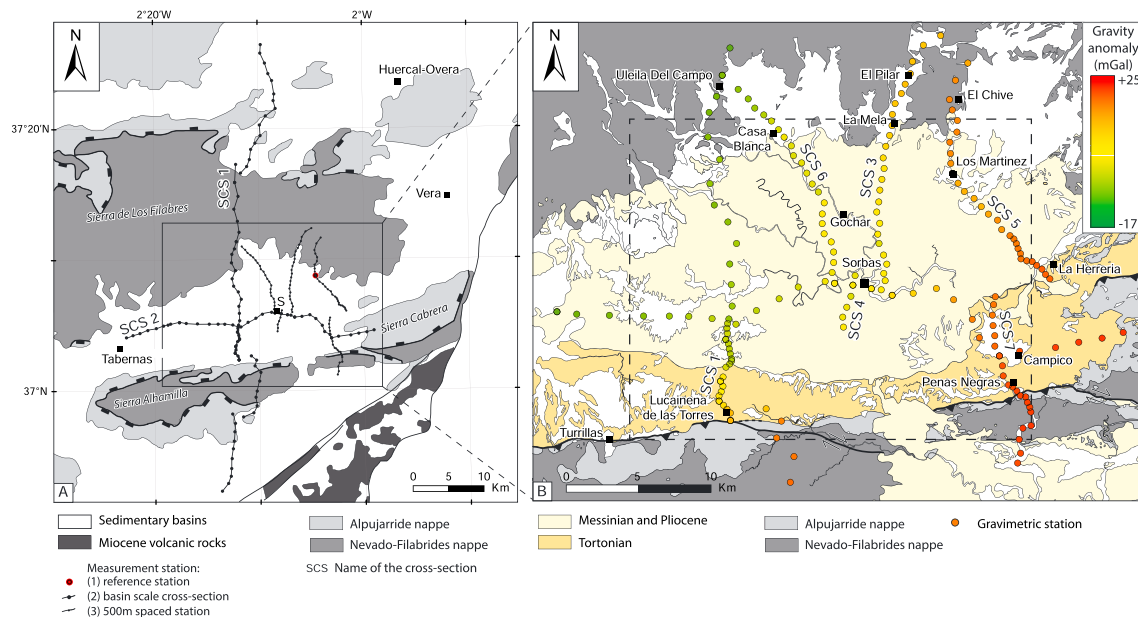


**Figure 7.** (a) Simplified geological map showing gravimetric cross sections realized across the basin. Red circle represents the reference station. (b) Location of the gravimetric stations and gravity anomaly plotted over the geological map of the Sorbas Basin. All measurement stations are represented by small circles colored in function of their relative Bouguer anomaly (see the color bar in the upper right corner). The dashed border rectangle represents the extension of the modeling box used to model in 3-D the sediments/basement interface at depth.

density was chosen as an average density value for crustal rocks. Inner terrain corrections (for 50 m of distance away from station) were routinely performed using *Hammer charts* [1939]. Following *Martelet et al.* [2002], far field terrain corrections (up to 167 km away from the station) were computed numerically using the Shuttle Radar Topography Mission digital elevation model. Finally, the Bouguer anomaly values were calibrated (with a constant shift) to the available regional-scale gravity data [*Torne et al.*, 2000] in order to refer to a common and absolute gravity reference with other existing data sets (see Figure 8a).

Two dimensional (2-D) direct gravity modeling was performed using the Geosoft-GM-SYS software. Gravity Bouguer anomalies depend on both the geometry and the density contrasts between geological units. In order to avoid multiresolution models from the gravity analysis, densities of the geological units were measured at the laboratory using the hydrostatic weighing method. Densities used for each lithology considered in the model are listed in Table 1 and detailed below. These were also systematically compared to published density range values usually considered for classical lithologies [*Robinson and Çoruh*, 1988; *Telford et al.*, 1990; *Jacoby and Smilde*, 2009]. While density values were fixed, the modeling process then consisted to adjust geometries of the geological units along the sections. The Moho depth variation generally induces large-wavelength variations in gravity anomaly profiles, and, for this study, the geometry of this particular interface is fixed from the available reference data set of *Fullea et al.* [2006] or *Ziegler and Dèzes* [2006]. The geometry of each geological unit was drawn in accordance to the geological maps [*García Monzón et al.*, 1973b, 1974] (Figure 2).

### 6.2. Rock Densities

Rock densities were directly measured from several rock samples for each geological unit. Indeed, the determination of average standard densities for a geological formation highly depends on the definition of the lithological assemblage [*Jacoby and Smilde*, 2009]. Gravity modeling based on measured densities ensures a much better control. Both the Alpujarride and the Nevado-Filabride complexes metamorphic basement were sampled (Figure 2). The purple micaschists of the Alpujarride complex were sampled near Lucainena de Las Torres at the southern edge of the basin. The corresponding measured density ( $2.69 \text{ g cm}^{-3}$ ; see Table 1) is consistent with the general bulk densities usually considered for micaschists and phyllites (i.e., from  $2.64$  to  $2.74 \text{ g cm}^{-3}$ ) [*Jacoby and Smilde*, 2009]. Due to the occurrence of dolomitic layers at all scales, the density of the Triassic metacarbonate rocks from the upper part of the Alpujarride complex was fixed from the literature [e.g., *Jacoby and Smilde*, 2009] with a bulk density of  $2.7 \pm 0.2 \text{ g cm}^{-3}$ . An average density of  $2.69 \text{ g cm}^{-3}$  was thus attributed to the overall Alpujarride complex for modeling. Micaschists samples of all three units

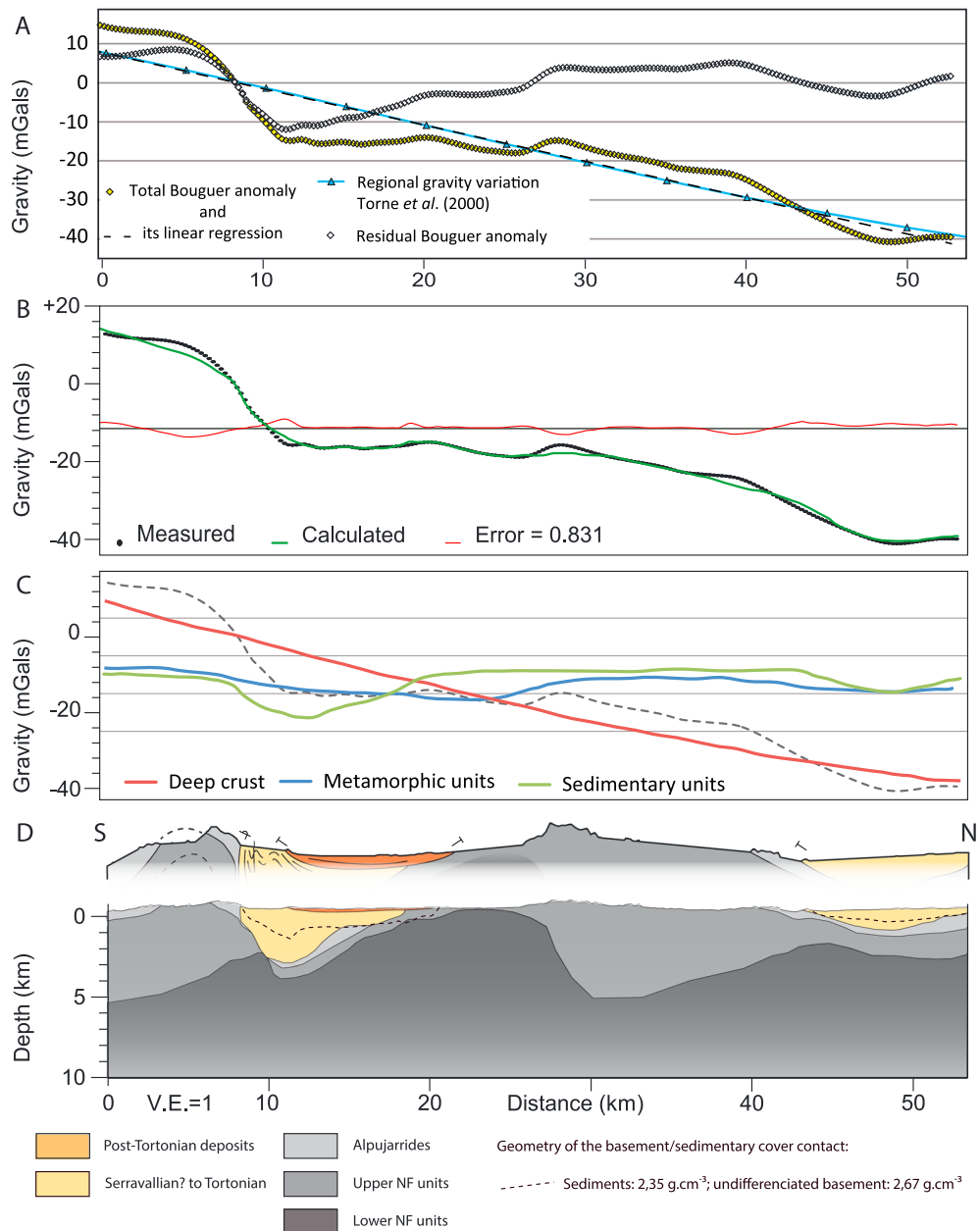


**Figure 8.** Two-dimensional gravity profile treatment. (a) Comparison between the measured total Bouguer anomaly (yellow diamond shape) and the regional gravity deviation exposed in *Torne et al.* [2000] of the N-S regional cross-section (SCS1). White diamond-shaped points represent the calculated residual gravity anomaly profile (see text for details). (b) Superposition of the 2-D gravity model anomaly (green curve), calculated from the density summarized in Table 1, with the measured total Bouguer anomaly (black dots). The red curves correspond to the difference between the modeled gravity anomaly and the measured one. (c) Deconvolution of the measured gravity signal (black dashed line) showing the combined effects of the deep structures of the crust and more particularly the Moho geometry (red curve); the upper crust structure of the outcropping metamorphic units (blue curve) and the shape and thickness of the sedimentary basins (green curve). (d) Shallow field based cross section and interpretation of the modeled 2-D gravity anomaly across the Sorbas basin. Note the strong asymmetry of the sedimentary depocenter.

composing the Nevado-Filabride complex (i.e., the Ragua Unit, the Calar-Alto Unit, and the Bédar-Macael Unit) yielded densities of 2.65, 2.67, and 2.69 g cm<sup>-3</sup> respectively (Table 1). These densities are in good agreement with both average densities published in the literature [*Jacoby and Smilde, 2009*] and the fact that the metamorphic grade of these complexes increases in this same order. Indeed, despite a relatively common lithological succession, one main distinction between those units is ascribed to the presence of metabasite

**Table 1.** Sampling and Density Measurements

Sedimentary units	Lithologies	N° Sample	Density		
			Measured	Reference	Literature
Latest Messinian	Fluvial conglomerates			2.36	
Early Pliocene	Coarse-grained conglomerate	1	2.4	2.36	Limestone: $2.49 \pm 0.12$
Gilbert delta	Marls and clays	2	2.32		Marl: $2.40 \pm 0.10$ ; clay marl: $2.06 \pm 0.3$
Messinian evaporites	Gypsum	3	2.31	2.31	Gypsum: $2.35 \pm 1.5, 2.5$
Messinian reef and marls	Reef	4	1.82	2.4	Marl: $2.40 \pm 0.10$
	Whitish diatomite and laminite	5	1.47		
Lowermost Messinian	Rich fossiliferous calcarenite	6	2.46	2.46	Conglomeratic limestone: 2.48
Tortonian turbiditic	Sandstone	7	2.54	2.54	
Alpujarride nappe	Purple schists	8	2.69	2.69	Schist: $2.64 \pm 0.26$
Bedar-Macael unit	Nevado-Filabride complex				
	Lubrin granite, marble	9	2.67	2.9	Amphibolite: $2.96 \pm 0.8$ ; eclogite: $3.37 \pm 0.17$
Calar-Alto unit	Graphitic and black schists	10	2.67	2.67	Gneiss, schist: $2.65 \pm 0.25, 0.35$
Ragua unit	Black schists		2.65	2.65	Phyllite: $2.74 \pm 0.60$

bodies in both Bédar-Macael and Calar-Alto units (which include eclogite and amphibolite rocks) that were not directly measured [García Monzón *et al.*, 1973a; Martínez-Martínez and Azañón, 1997]. Average densities of such basic rocks are respectively about 3.3 and 2.9 g cm<sup>-3</sup> [Jacoby and Smilde, 2009]. Hence, the adjacent Bedar-Macael and Calar-Alto units have been considered as a single unit for gravity modeling, hereafter called the Upper NF unit, with a slightly increased average density of 2.7 g cm<sup>-3</sup> (Table 1). The lowermost metamorphic unit has been defined as the Lower NF unit (corresponding to the above mentioned Ragua Unit) with a measured average density value of 2.65 g cm<sup>-3</sup>. On the regional-scale cross-section SCS1 (Figure 7a), the use of dense bodies was not necessary to adjust the modeled residual Bouguer anomaly with the measured one. At that scale, far-field effects of these scarce and dense bodies can be neglected. On the contrary, adjustment of the modeled residual Bouguer anomaly on small-scale cross-sections required the use of such bodies, in accordance with their exposures [García Monzón *et al.*, 1973b, 1974].

Sampling of the sedimentary cover has been performed throughout the entire basin (Figure 2). Apart conglomeratic layers (from the upper Serravallian to lower Tortonian), whose density cannot be obtained by laboratory measurement, densities of all the sedimentary units have been measured (see Table 1). Two groups have been distinguished for modeling: one including Serravallian and Tortonian deposits and another one from lowermost Messinian to uppermost Pliocene layers. The average density obtained for Tortonian deep marine deposits (2.54 g cm<sup>-3</sup>; Table 1) has directly been used in the 2-D modeling process. Densities measured for the lowermost calcarenite, Messinian marls-reefs-evaporites, and the overlying latest Messinian to early Pliocene deltaic deposits are summarized in Table 1. The density measured for the Messinian marls, yielding a density of 1.6 presents much lower values than the density usually considered for such rock type (2.4 g.cm<sup>-3</sup>) [Jacoby and Smilde, 2009]. Consequently, and in order not to unbalance the gravity modeling, an average density of 2.4 g cm<sup>-3</sup> has been considered for his unit. Finally, a mean 2.37 g cm<sup>-3</sup> density has been calculated for the entire lowermost Messinian to uppermost Pliocene group. Note that the density of the topmost Pliocene conglomeratic layers has not been measured because of their sample-scale lithological heterogeneity and their noncohesive structure. It has been considered equal to the Pliocene marine deposits, which yielded averaged density of 2.36 g cm<sup>-3</sup>.

### 6.3. Gravity Profiles Modeling

A 55 km long profile, crossing the Sierra Alhamilla to the South and the Sierra de Los Filabres to the North, was acquired to image the effect of the overall crustal structure on the gravity signal (Figure 8). Indeed, wavelength of the gravity anomaly primarily depends on the depth (for given density contrasts) of the “source” geological bodies and structures; rather long profiles are thus required to image the deepest crustal geometries. Here, the long N-S Bouguer anomaly profile, hereafter named the “regional-scale” profile, shows a large northward decrease from +15.15 mGal to -42.10 mGal (Figure 8a); this long-wavelength anomaly corresponds to the regional gravity anomaly and, at first order, this can be related to a north dipping Moho (Figure 8b). This feature is in good agreement with the Moho depth model/compilation published by Ziegler and Dèzes [2006] or Díaz and Gallart [2009] showing a progressive northward deepening, from 22 km to 32 km, beneath the Sierra de Los Filabres.

The residual Bouguer anomaly values corresponding to this regional profile (Figure 8) were calculated by subtracting the measured Bouguer anomaly and the regional Bouguer anomaly as given by *Torne et al.* [2000] or *Fullea et al.* [2010]. The obtained profile then appeared very similar to the one recently published by *Li et al.* [2012]—who surveyed approximately the same regional-scale section—with similar amplitudes and shapes of the two residual Bouguer anomaly curves (compare Figure 8a and *Li et al.* [2012, Figure 3]). As the two surveys and studies have been strictly conducted independently, such features highlight a good reproducibility of the measurements and treatments and the quality of the gravity data used for this study. Here all the 2-D gravity models were computed from the “total” Bouguer anomaly values (instead than from the residual Bouguer anomaly) by taking into account the geometry of the Moho, as mentioned above [*Torne et al.*, 2000; *Fullea et al.*, 2006; *Ziegler and Dèzes*, 2006]. It is noteworthy that, below the lowermost NF metamorphic unit, standard densities have been used for the crust with 2.7 and 2.8 g cm<sup>-3</sup> for respectively the “mean” and lower crust levels.

On the other hand, short wavelengths of the measured gravity profiles highly depend on the shallow crustal structure. In this study, this part of the modeling was constrained by the geometry of the outcropping post-Tortonian deposits within the Sorbas basin (see Figure 2) and of the metamorphic unit, into the domes, as deduced from field structural measurements. The midwavelength anomaly (Figure 8a) constituted the only remnant part of the measured signal to be fitted. If considering the density contrast in between units (see Table 1), the latter depends not only on the depth and shape of the base of the basin but also on the geometry of internal boundaries within the underlying metamorphic complexes (Figure 8b). The residual midwavelength anomaly was then modeled by adjusting the geometry of the contact between metamorphic basement and sediments (Figure 8b), as is the case to the northern boundary of the basin (Figure 8c). As a whole, the modeled Bouguer anomaly can be separated in three components along this regional-scale profile (see Figure 8c), displaying the combined effects of (i) the deep crustal structures (red curve), (ii) the upper crust structure into the outcropping metamorphic units (blue curve), and (iii) the shape and thickness of sedimentary basins (green curve in Figure 8c). Note that, even though a large part of the total Bouguer anomaly range value is directly linked to the Moho depth (see red curve in Figure 8c), a significant part of its variations is also due to the structure of the upper crust of both the metamorphic and sedimentary units, with similar proportions (see similar amplitudes of the blue and green curves in Figure 8c). Finally, on the regional-scale SCS1 profile, the midwavelength Bouguer anomaly decreases from 5 to 25 km, which corresponds to an asymmetric shape of the basin floor as shown in the model (Figure 8d).

Profiles SCS3, SCS4, SCS5, SCS6, and SCS7 (Figure 7), located in the center of the Sorbas basin, are described from West to East (Figure 9). In comparison to the above described ~55 km long regional-scale profile, the latter shorter profiles stand for more local-scale variations in the structure of the basin. For the sake of clarity, modeled geometries of the units are only displayed down to 4 km on the sections but, as for the processing of SCS1 profile, the whole crust is taken into account for gravity anomaly computation, down to the mantle, in order to include depth variations of the Moho. Profile SCS6 extends to the North from Uleila del Campo to the west of Sorbas city (Figure 7). The short wavelengths of the Bouguer anomaly are well fitted by taking into account the extension of the northern boundary of the Tortonian trough beneath the Messinian and Pliocene sediments (see Figure 2). On the other hand, the gravity high displayed in the Bouguer profile (between 2 and 4 km) and forming a midwavelength anomaly cannot be simply reproduced by the presence of standard metamorphic rock units below the post-Tortonian deposits. Such wavelength can neither be explained by variations in the Moho depth nor in the lower crust. Gravity modeling shows here that the occurrence of rather dense material (of 2.9 g cm<sup>-3</sup>) in the upper crust is mandatory, at that local-scale, to properly model the Bouguer gravity anomaly. Slices of such dense rocks are displayed in black in Figure 9. Note that such small bodies are only necessary to adjust short wavelength of the anomaly in “local” gravity profiles and are not mandatory for modeling the regional-scale profile as described above. SCS4 profile, which extends 3 km south of Sorbas, is the southern extension of the SCS6 profile. The first-order trend of the modeled Bouguer anomaly was adjusted with the geometry of the metamorphic basement units at depth. Shortest wavelengths have been then modeled with the depth of the interfaces of shallow geological units exposed at the surface. SCS3 profile is almost parallel to SCS6 and extends from Sorbas to the north of El Pilar (Figure 7). The same modeling protocol as described above was used here to adjust the computed Bouguer anomaly curve to the measured anomaly values. Here again, this section displays the extension of the northern boundary of the Tortonian trough below the younger sedimentary series. The N-S oriented SCS7 profile extends

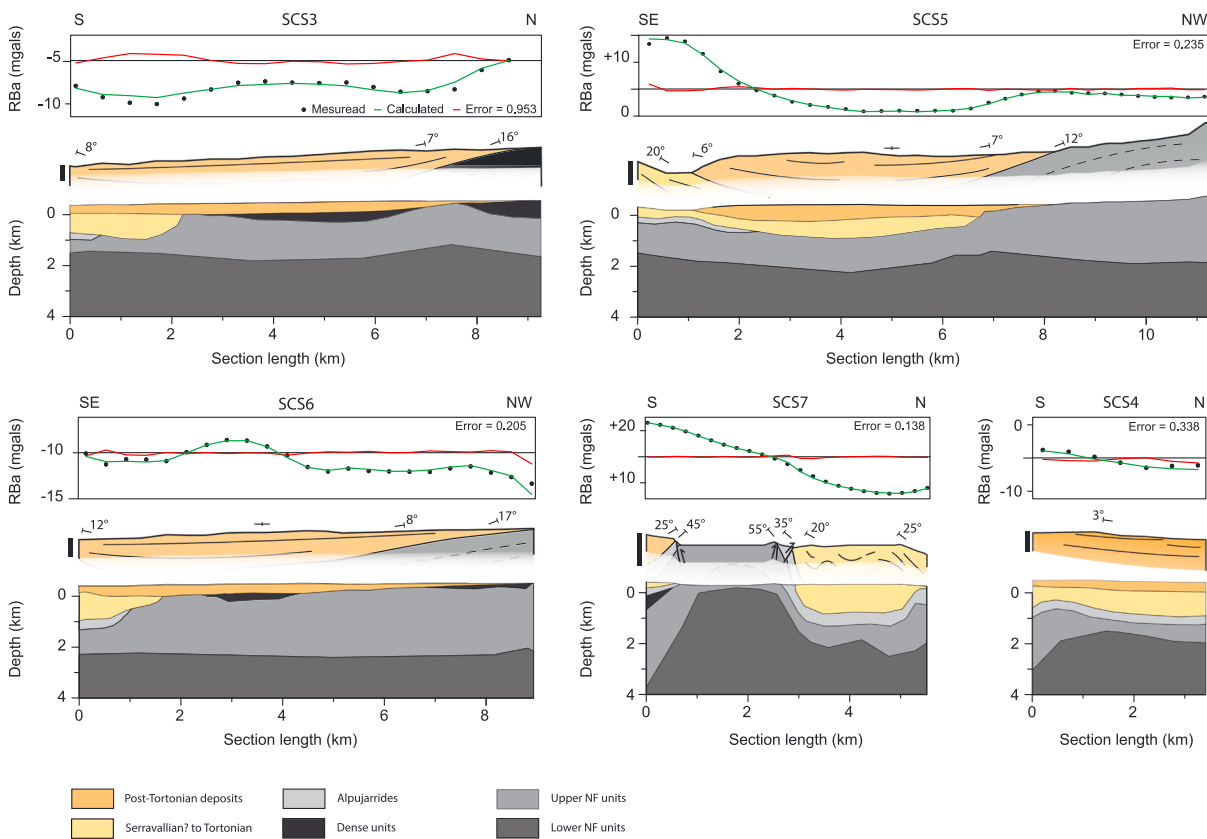


**Figure 9.** Total gravity anomaly, shallow field-based cross section and corresponding 2-D model constructed for the five cross sections called SCS3 to SCS7. The gravity modeling of these cross sections is equal to that detailed in the text for the basin-scale SCS1 cross section. Vertical exaggeration = 2; see Figure 7 for location.

from Los Feos (northern part of the Nijar basin) to Los Perales (Figure 7). This profile crosses a metamorphic basement high connecting the Sierra Alhamilla in the west to the Sierra Cabrera in the east and where metamorphic rocks have been sampled to constrain density values (Figure 2). The northward decrease of the Bouguer anomaly values, from +21 to +8 mGal (Figure 9), was ascribed to the anticline shape of the metamorphic units as known laterally in both Sierra Alhamilla and Sierra Cabrera. At 2.8 km distance along the profile, a trend break is visible in the anomaly curve, and this feature most probably coincides with the basement/sediments contact outcropping there (Figure 9). This argues for a rather steep downward extension of the contact. Besides, the sedimentary cover is here entirely composed of Tortonian sediments, and this structure may correspond to the termination of the Tortonian extensional trough to the SE. The westernmost gravity section extends from La Herreria to north of El Chive (SCS5 profile; Figure 7). Three main segments can be distinguished along the Bouguer anomaly profile: (a) the first one, between kilometer 0 and 2, is characterized by a northwestward strong decrease; the best fit of the model was obtained by an important deepening of the sedimentary infill of the basin; (b) the second segment, between 2 and 7 km, is marked by a rather constant low anomaly which corresponds, after adjusting the model, to the thickest sediment filling along the cross section; and (c) the third segment, beyond 7 km, highlights a rather weak increase of the anomaly before a new stabilization around +3 mGal. This “step” in the trend of the Bouguer anomaly profile may correspond to the extent of the Upper NF units from the Sierra de Los Filabres southward below the post-Tortonian series (Figures 2 and 7). Except for the extreme northern boundary of the SCS6 profile, the measured and modeled Bouguer anomalies show a good consistency, and the resulting misfit error is negligible for all profiles.

### 7. Three-Dimensional Geometry and Depth Constraints

Two-dimensional gravity sections were integrated into the 3-D *GeoModeller* software [Calcagno et al., 2008; Guillen et al., 2008] in order to interpolate the 3-D geometry of the basin floor. The computation principles of

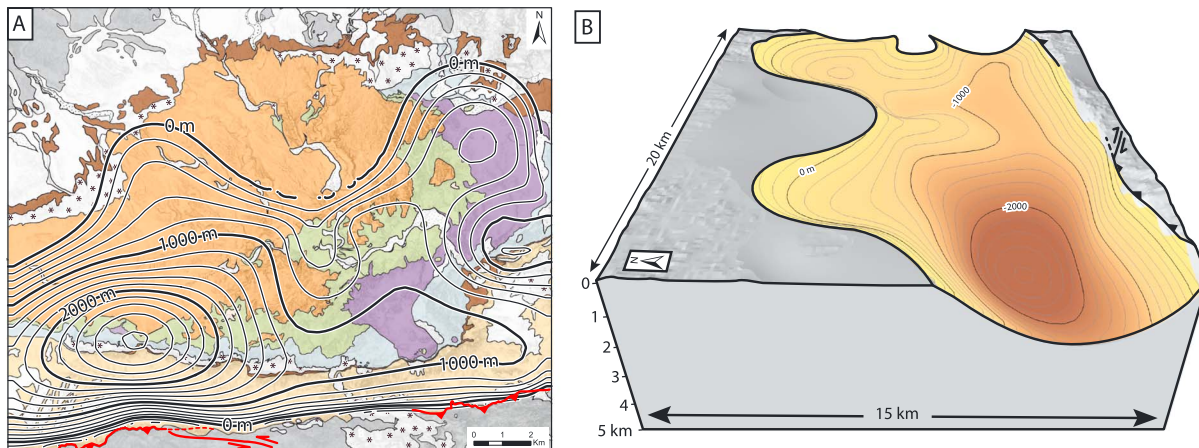


**Figure 10.** Basin floor 3-D geometry. (a) Isodepth curves of the base of the Tortonian deposits are plotted over the geological map of the modeled area. The depth is indicated in meters below sea floor. (b) Three-dimensional oblique view of the base of the Sorbas basin. Vertical exaggeration = 3.

this software are based on a joint inversion of both the places, within the 3-D volume considered, where geological contacts have been observed or deduced, and measured orientations of corresponding geological surfaces. Here modeled 2-D gravity sections were thus used to constrain both the depth of the basin floor and its geometry. The modeling box (dashed border rectangle in Figure 7b) extends over  $20 \times 15$  km from  $37^{\circ}10'12.33''\text{N}$ – $2^{\circ}15'03.00''\text{W}$  (top left corner) to  $37^{\circ}01'48.44''\text{N}$ – $2^{\circ}02'12.75''\text{W}$  (bottom right corner) and from 5 km below sea level to 3 km in altitude.

The geometry of the basin floor is illustrated in Figure 10 by both an isodepth curve map (Figure 10a) and an oblique 3-D view of the model in which the sediment infill have been removed (Figure 10b). Isodepth curves of the basin floor, as interpolated during the 3-D modeling process, show a strong marked asymmetry of the basin geometry (Figure 10a) characterized by a steep North dipping boundary in the southern part of the basin, passing to a gently South dipping contact to the North. This first-order geometry of the model is well constrained by both (i) the gravity 2-D modeling along the profiles and (ii) the very steep dip of the first Tortonian layers even characterized by locally overturned bedding close to the basement contact. The deepest part of the basin, a 2000–2800 m trough, is located in the South, facing the North Alhamilla front zone separating the basin from the metamorphic basement of the Sierra Alhamilla.

While the asymmetrical shape of the basin evidenced by our computed 3-D model is compatible with the 2-D image proposed by *Li et al.* [2012], discrepancies arise when considering the modeled depth of the basement/sediment basement below the basin. Indeed, previous work estimates a  $\sim 1500$  m maximum depth of the Sorbas basin in its southern part, whereas our 3-D computations result in a 2000–2800 m depth localized along the southern part of the basin. When considering the SCS1 regional-scale gravity section of this study, comparison of the residual Bouguer anomaly values with the one obtained by *Li et al.* [2012] clearly shows that such discrepancy could not be attributed to measurement deviations. Thus, differences in depth computations must be assigned to the choice of the density values used for gravity modeling. On the one hand, previous gravity studies conducted in the Sorbas basin and surrounding areas gathered geological units in, basically, two groups (i) sedimentary rocks with a constant density fixed at  $2.35 \text{ g cm}^{-3}$  and (ii) basement rocks with a constant density fixed at  $2.67 \text{ g cm}^{-3}$  [*Pedraza et al.*, 2009, 2010; *Li et al.*, 2012]. We have tested this same approach on the N-S regional cross section to model the basal contact separating the sediments from the metamorphic basement (dashed line on Figure 8d). The overall asymmetric shape of the basin fill can be reproduced; however, the main difference between these approaches is the resulting depth of the basin floor estimated between 1.6 to 2.8 km (Figure 8d). However, the Bouguer anomaly primarily depends on density contrasts [*Martelet*, 1999; *Martelet et al.*, 2004; *Jacoby and Smilde*, 2009; *Joly et al.*, 2009]. Accurate determination of the density is thus essential to model a more reliable geometry to depth. The Sorbas basin, as well as its basement, is composed of a large spectrum of rocks and average densities assigned to each geological layer sufficiently contrasts with both adjacent units to be considered as a representative density interval (Table 1). Our study strives to consider more specific density values for geological units or groups as

recognized in the area as well as measuring densities from field samples rather than using standard average density values. When comparing densities of rock units measured in this study to standard ones, we suggest that the distinction of as many geological units as possible to separate “geophysical” units is a more accurate approach to estimate both the geometries and depths of the geological boundaries.

## 8. Discussion

Contrasted tectonic settings have previously been proposed to explain the initiation and the development of sedimentation within the Sorbas basin: (i) N-S compression to transpression [Montenat *et al.*, 1987; Weijermars *et al.*, 1985; Ott d'Estevou *et al.*, 1990; Sanz de Galdeano and Vera, 1992; Poisson *et al.*, 1999], including strike-slip tectonics [Kleverlaan, 1989; Haughton, 2001], or (ii) extension [García-Dueñas *et al.*, 1992; Vissers *et al.*, 1995; Martínez-Martínez and Azañón, 1997; Augier *et al.*, 2005a, 2013]. Based on field structural investigations and the gravity survey, the 3-D geometrical model shows a marked asymmetric shape with the deepest parts localized to the South, along the contact with the Sierra Alhamilla. The southern basin/basement rocks contact is steeply dipping, so as the bedding within the Tortonian basal deposits. The southern deepest parts of the basin correspond to the Tortonian trough, as previously defined. The strong asymmetry of the basin might result from the compressive event, when the Sierra Alhamilla “thrust” over the southern edge of the Sorbas basin. Indeed, the North Alhamilla Reverse Fault has been described as a prominent structure, and its development could have been accompanied by a significant subsidence in its footwall. However, structural analysis highlighted that while north verging thrusting can be evidenced along this margin, some segments of the north Alhamilla front display a preserved structure of unconformable stratigraphic contact of the Tortonian series on the basement rock units. Such interface was subsequently tilted or even overturned in front of the Sierra Alhamilla but no trace of thrusting can be evidenced then. In these areas (as presented in Figure 4) the deformation marks the growth of a fault-propagated fold at the tip of a blind thrust, and such quick change in tectonic style along the north Alhamilla front argues for a rather limited dip slip movements along the NARF. On the other hand, while previous works estimate ~1500 m of maximum depth for the Sorbas basin, our new gravimetric models and 3-D computations result in a 2000–2800 m maximum depth localized along the southern part of the basin. This result reinforced the asymmetric character of this basin. It also highlights a much larger cumulated subsidence in this area compared to the Huércal-Overa basin for instance.

Moreover, several synsedimentary normal faults have been locally described from the upper Serravallian to the upper Tortonian series, in close surroundings to the Sorbas basin (Figures 5 and 6). Two extensional paleostresses, whose minimum compression direction [ $\sigma_3$ ] are N140E and N50–60E oriented, controlled the deposition of upper Serravallian to upper Tortonian sediments (Figures 5 and 6). The analysis of upper Tortonian series, in particular in the Gafarillos area, suggests that the N140E oriented system was mainly restricted to the upper Serravallian to early Tortonian. In the Tabernas area, both normal faults sets appear clearly as prefolding extensional faulting as suggested by tilted conjugate sets of normal faults (Figures 6b and 6c). The asymmetry of the basin floor most probably results from the successive extensional and compressive deformations evidenced in the Sorbas basin. Indeed, the limited dip-slip movements along the northern “thrust” front of the Sierra Alhamilla could hardly explain the ~2500 m of subsidence in the south Sorbas trough. In addition, the amount of shortening due to the folding of the Alhamilla range remains hardly assessable because of the dextral movements of the Polopos and North Alhamilla Fault Zone [Jonk and Biermann, 2002; Giaconia *et al.*, 2012a] and the involvement of the strike-slip Cantona Fault Zone in the deformation [Haughton, 2001]. Therefore, we assume that a significant imprint of the early extensional event contributed on the finite global architecture and structure of the Sorbas basin.

### 8.1. The Initial Extension History of the Sorbas Basin and Surroundings

The onset of sedimentation roughly occurred at the same time in all intramontane basins of SE Betics, during upper Serravallian to lower Tortonian [Cloetingh *et al.*, 1992; Sanz de Galdeano and Vera, 1992; Iribarren *et al.*, 2009]. The Huércal-Overa and Sorbas basins underwent a common subsidence history during their early development stage (Figure 11): this first phase is characterized, in both basins, by the deposition of a thick coarse-grained breccia containing Nevado-Filabride clasts [Sanz de Galdeano and Vera, 1992]. Both basins display a synchronous onset and a similar evolution of sedimentation [Sanz de Galdeano and Vera, 1992], while their basement were exhumed by normal faulting. Evidences of extensional tectonics during the lower

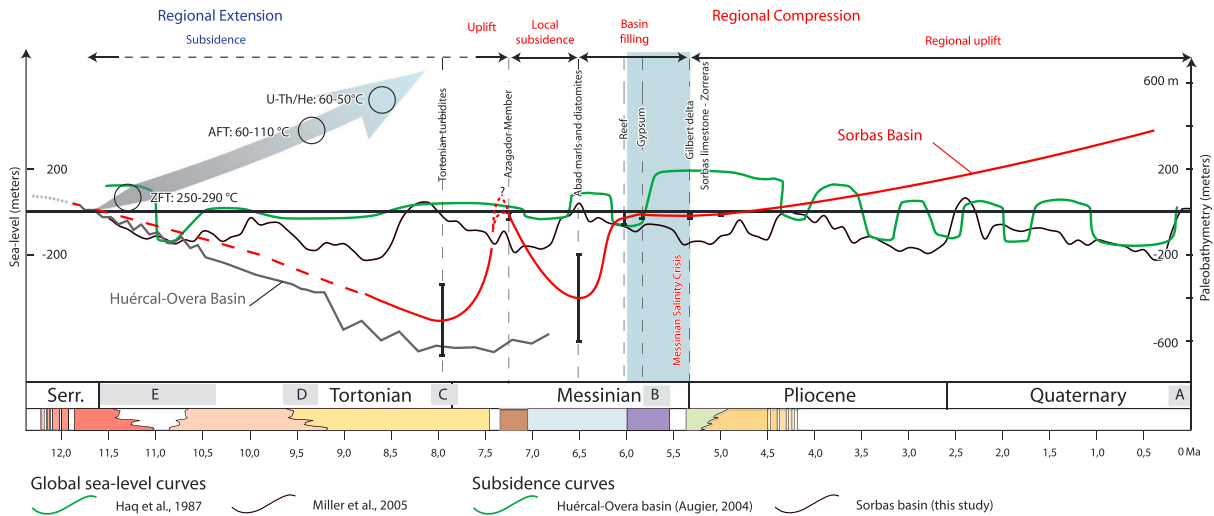


**Figure 11.** Tectonic subsidence and uplift curves for the Sorbas and the Huércal-Overa basins during the Neogene (thick black and red curves, respectively). The subsidence curve of the Sorbas basin is drawn from the average estimated paleobathymetries compiled in Table 2. Absolute eustatic curves are from *Haq et al.* [1987] and *Miller et al.* [2005]. Exhumation and cooling path of the Nevado-Filabrides complex are estimated from ZFT, AFT, and U-Th/He methodologies [*Johnson et al.*, 1997; *Augier et al.*, 2005b; *Platt et al.*, 2005; *Vázquez et al.*, 2011]. Grey rectangles noted A to E refer to steps of the evolutive cross section of the Sorbas basin in Figure 13.

Tortonian have also been extensively described into the Huércal-Overa basin, to the north (Figure 12a) [*Briend et al.*, 1990; *Augier et al.*, 2005b; *Meijninger and Vissers*, 2006; *Pedraza et al.*, 2010; *Augier et al.*, 2013]. In that area, the latest exhumation stages of the metamorphic Nevado-Filabride complex (green arrows in Figure 12a) [*Johnson et al.*, 1997; *Augier et al.*, 2005b] coincide with the kinematics of normal faults which controlled the sedimentation into the basin [*Augier et al.*, 2013]. Both basins may have experienced common extensional tectonics during the initiation of sedimentation (Figure 12a). The effect of extension is obviously hardly detectable on the southern edge of the Sorbas basin. However, similar extensional regime-bearing metamorphic core complexes in other surrounding areas led to the formation of half-graben basin such as the Granada basin [*Ruano et al.*, 2004], Fortuna-Guadalestín basins [*Amores et al.*, 2001, 2002], and in the Alboran Sea [*Mauffret et al.*, 1992; *Watts et al.*, 1993; *Comas et al.*, 1999]. We assume that the Sorbas basin which initiated under similar tectonic conditions (Figure 12) may have formed an asymmetric half graben tilted toward the south. The fact that extensional paleostresses calculated in this study, and especially the N140E oriented system, is consistent with the latest ductile deformation highlighted in the Sierra Alhamilla (green arrows in Figure 12a) reinforces the comparison with the Huércal-Overa basin and the interpretation of half-graben initiation. In the Sorbas basin, gravity modeling evidences that the rather dense rocks of the Alpujarride complex with respect to the sedimentary cover, cannot be prolonged northward, below the basin (Figures 9 and 13e), without inducing a large misfit on the measured Bouguer anomaly. Hence, the southern fault which probably controlled the sediments deposition during the initiation of the subsidence may crosscut and postdate the Alhamilla detachment zone itself (Figure 13e). This is fairly consistent with the tectonic history of the Huércal-Overa basin and the circa 12–11 Ma ages for the initiation of sedimentation during latest exhumation stages of the sierras under brittle conditions [*Platt et al.*, 2005].

**Table 2.** Paleobathymetry and Age of the Sedimentary Formations of the Sorbas Basin

Formation	Age	Paleobathymetry (m)	References
Zorreras coquina	≈ 5.2 Ma	20 m	<i>Montenat et Ott d'Estevou</i> [1977]
Sorbas calcarenite	5.67–5.60 Ma	20–40 m	<i>Montenat et al.</i> [1980]
Gypsum	5.97–5.67 Ma	0–40 m	<i>Dronkert</i> [1976]; <i>Goubert et al.</i> [2001]
Messinian reef	6.04–5.89 Ma	0–80 m	<i>Braga et al.</i> [2003]; <i>Sanchez-Almazo et al.</i> [2007]
Abad marls	7.24–5.96 Ma	200–600 m	<i>Dronkert</i> [1976]; <i>Troelstra et al.</i> [1980]; <i>Ott d'Estevou and Montenat</i> [1990]; <i>Poisson et al.</i> [1999]; <i>Krijgsman et al.</i> [2001]
Tort/Mess calcarenites	≈ 7.24 Ma	20–40 m	<i>Ott d'Estevou and Montenat</i> [1990].
Upper Tortonian	> 7.24 Ma	350–600 m	<i>Ott d'Estevou et al.</i> [1981]

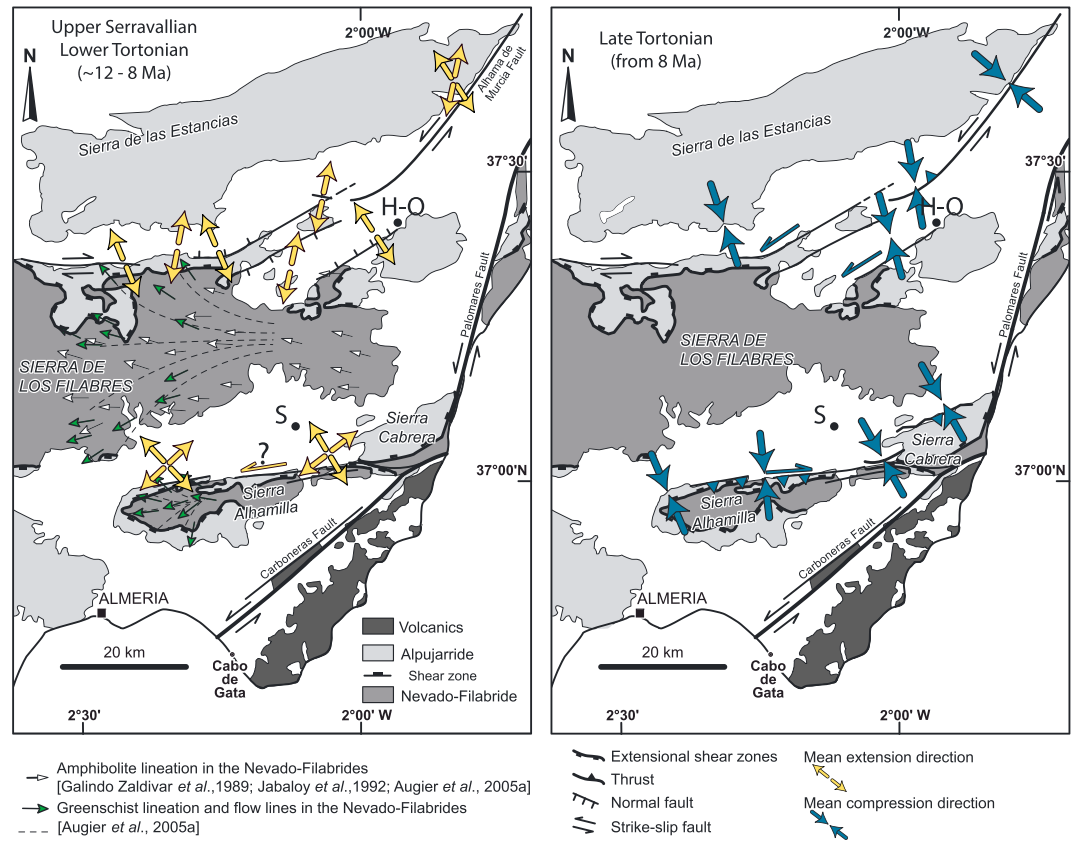


**Figure 12.** Simplified tectonic map showing average upper Serravallian-lower Tortonian extension directions and average upper Tortonian compressive directions of the southeastern part of the Internal Zones of the Betic Cordillera. Stretching direction and associated sense of shear for the Nevado-Filabride complex are synthesized from [Galindo-Zaldívar *et al.*, 1989; Jabaloy *et al.*, 1992; Augier *et al.*, 2005a]; Extension and compression directions shown in the Huércal-Overa basin are derived from Meijninger [2006] and Augier *et al.* [2013].

### 8.2. Evolutive Scenario of the Sorbas Basin

A N-S evolutive cross section of the Sorbas basin is given in Figure 13. Situations are restored for key main steps from the upper Serravallian to lower Tortonian stage to the present view by deconvoluting the tectonic history of the Sorbas basin. As discussed before, we argue here for an onset of sedimentation occurring in an extensional regime in the Sorbas basin. The strong asymmetry of the basin is compatible with a half-graben geometry controlled by a supposed north dipping fault zone, located along the southern margin during Serravallian and part of the Tortonian (Figures 5 and 6). Geometry and major bounding faults of this initial basin can obviously not be retrieved accurately as most of this basin is now hidden by younger deposits; a significant part of the early basin even being eroded in particular during Messinian evolution. Extensional kinematics, as studied within the preserved and outcropping parts of the basins, is compatible with a NW-SE (~N140E) and NE-SW (~N50–60E) directed subhorizontal extension accompanied by a subvertical maximum compression direction (Figure 6). This event may have favored an initial subsidence pulse and the deposition of coarse-grained sediments grading to marine deposits. Such pulse thus seems recorded over most the SE Betic basins [Sanz de Galdeano and Vera, 1992; Meijninger and Vissers, 2006; Augier *et al.*, 2013]. Inception of the main sedimentation occurred shortly after the crossing of the ductile-brittle transition at circa 14–13 Ma during the final exhumation and the denudation of the Nevado-Filabride-cored domes [Johnson *et al.*, 1997; Augier *et al.*, 2005b; Vázquez *et al.*, 2011]. In the Huércal-Overa basin, where the corresponding oldest deposits are exposed and even very well preserved, this time interval corresponds to sedimentation of about 1 km thick series along the normal-faulted southern boundary [Pedrera *et al.*, 2009, 2010; Augier *et al.*, 2013]. As the two basins show a similar tectonic subsidence evolution during upper Serravallian to lower Tortonian, one can assume that, in the Sorbas basin, the subsidence pulse led reasonably to the deposition of the same amount sediments.

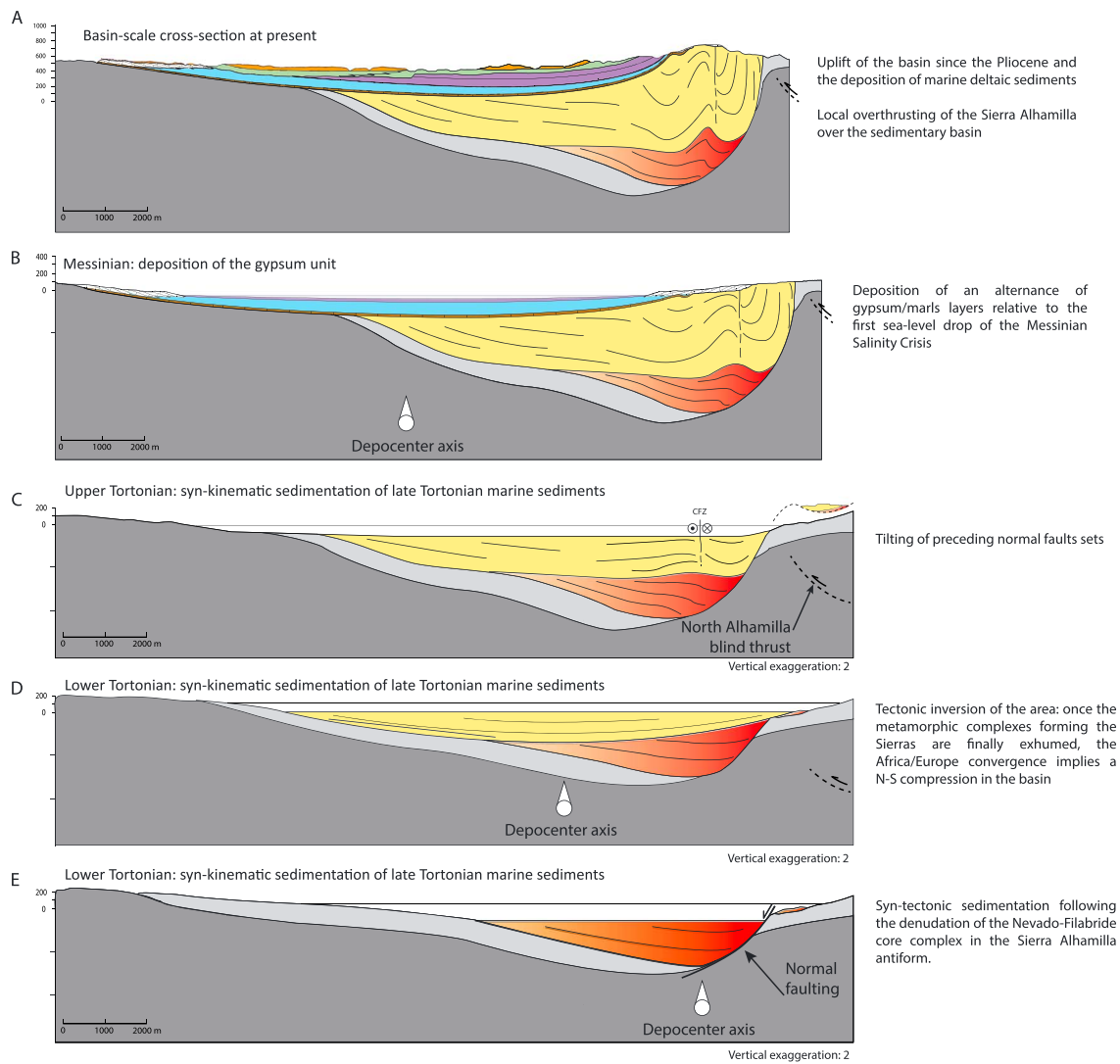


**Figure 13.** Interpretative N-S cross sections of the Sorbas basin representing its evolution from (a) the present to the deposition of (b) Messinian evaporites, (c) the late Tortonian syntectonic sedimentation of turbidites, and (d) the period of tectonic inversion postdating the extensive deformation during (e) the upper Serravallian to lower Tortonian.

Later, during the upper Tortonian, the Sorbas basin experienced a drastic inversion tectonics stage (Figures 4 and 6). This formation shows a progressive steepening over more than 2 km and is even overturned in the vicinity of the Sierra Alhamilla in the footwall of the North Alhamilla reverse fault zone (Figure 4). Besides, the development of upper Tortonian growth strata highlights that deformation occurred during sedimentation (Figure 4). Second order folding (e.g., the Tabernas fold) and small-scale faults are all consistent with a N-S to NW-SE shortening (Figures 4 and 6). Progressive steepening on the southern margin of the basin (i.e., the mobile border) and the significant uplift of the Sierra Alhamilla [Braga *et al.*, 2003] probably resulted in a continuous tectonic subsidence within the basin and the persistence of marine deposits [Weijermars *et al.*, 1985; Kleverlaan, 1989]. Flexural type subsidence then superimposed on the former extensional depocenter and migrated northward (Figure 13d). This marked inversion of the basin appears mechanically in agreement with the development of dextral strike-slip faults recognized at the western and eastern edges of the basin [Giaconia *et al.*, 2013].

Many studies pointed out an important strike-slip component of the northern and southern Alhamilla-Cabrera-faulted boundaries during the Tortonian [Martínez-Martínez *et al.*, 2006; Rutter *et al.*, 2012] leading to drainage captures [Mather, 2000; Giaconia *et al.*, 2012b, 2013]. In addition, several authors suggested that strike-slip tectonics parallel to the E-W depocenter have been important in the evolution of the Sorbas basin in particular during the Tortonian turbiditic filling [Ott d'Estevou and Montenat, 1990; Haughton, 2001]. This assumption is

mainly based on the occurrence of contained turbidites and a reversal location of its ponding depocenter in the late Tortonian [Haughton, 2001]. However, the initial sinistral strike-slip movement advanced by the authors cannot be observed in the basin due to its intense late deformation. The associated primary east flowing sedimentation could result from the first-step extension highlighted in this study. Moreover, the tilted-block geometry inferred by Haughton [2001] seems unrealistic with respect to the 2-D gravity inversion.

Compared to the Huércal-Overa basin, inversion tectonics appears much stronger in the Sorbas basin [Weijermars *et al.*, 1985; Augier *et al.*, 2013]. Onset of regional inversion has been proposed to approximately occur before the Tortonian/Messinian boundary (e.g., ~7.7 Ma) [Weijermars *et al.*, 1985]. Besides, inversion tectonics affecting the northern flank of the Sierra de Los Filabres occurred roughly at the same time, around 8.2 Ma [Augier, 2004]. This period coincides in a broad sense with a period of geodynamic reorganizations of the southeastern Betics (Figure 12b) as described throughout the Alboran region, around 8 Ma [Comas *et al.*, 1999; Jolivet *et al.*, 2006].

At the Tortonian-Messinian transition, the basin experienced an overall uplift and erosion as attested by the deposition of the Azagador shallow marine calcarenite over the upper Tortonian (Figures 4 and 13c). The large open-fold syncline of the lowermost Messinian calcarenite shows the relatively limited shortening deformation affecting the basin after its deposition (Figure 13b). From that period, and despite a global sea level fall of 35 m [Haq *et al.*, 1987], deep marine marls were deposited into the Sorbas basin between 7.3 and 6.5 Ma (Figure 13b). The subsequent deposition of Messinian clays and diatomites, known as the Upper Abad Member, and of the coeval fringing reef, in a restricted marine environment, is once more coeval with a global sea level fall estimated at 60 to 70 m (Figure 10) [Haq *et al.*, 1987; Miller *et al.*, 2005]. These features highly suggest that the global eustatic variations have locally weaker effects on sedimentation than the tectonic control during the Sorbas basin tectonic inversion.

## 9. Conclusions

While most of the previous studies on Sorbas basin focused on the Messinian salinity crisis event or on compressive tectonics acting from middle-Tortonian to upper Tortonian times, this work aims at constraining the early tectonic context during the initiation phase of the basin. Two principal targets were identified as key points to address this problem: the geometry/structure of the early deposits with the basement units and the internal deformation/stress fields taking place during the onset and first stages of sedimentation into the basin. At first, structural analysis and compilation point out that the well-known northward thrusting movement observed along the northern edge of the Sierra Alhamilla may be limited; deformation being characterized by pervasive shearing and folding in some places. Besides, structural analysis of the earlier deposits along the southern margin of the basin, including computation of paleostress tensors from fault kinematics analysis, highlights the prime effect of an initial extensional event during the onset of basin development. This phase of deformation observed in sedimentary series is coeval with the late exhumation stages of the Nevado-Filabride complex, further south, into the Sierra Alhamilla, which is characterized by a top-to-the NW normal sense of shear [Augier *et al.*, 2005a]. This extensional context must probably controlled the inception of sedimentation in the continental basin.

On the other hand, gravity modeling revealed the deep and asymmetric structure of the Sorbas basin. This asymmetry is highlighted both by a gently south dipping basal unconformity in the north and a steep south dipping southern contact. Gravimetric survey and modeling results in the determination of a maximum ~2500 m of sediments accumulated and preserved along the southern margin of the basin. The Sorbas basin thus displays as a particularly thick basin in comparison to the other neighboring continental basins of the area, and its well-marked asymmetry could hardly be explained by the limited thrust movements as observed along the northern Sierra Alhamilla. All these results thus argue for a two stages evolution of the Sorbas basin development with (i) extension driving at first the initiation and first stages of subsidence and (ii) inversion of the basin and flexural control of the sedimentation during a subsequent compression.

Our integrated study allows estimating the evolution through time of the basin behavior. We propose that during the early extensional stage, a normal to normal-strike-slip fault system initiated the subsidence along the northern edge of the metamorphic range, south of the basin, during the last stages of exhumation of the metamorphic units. Later on, the asymmetry of the basin was reinforced during the basin inversion by the N-S compressional event occurring from circa 8 Ma. Since the deposition of the Azagador Member, the Sorbas basin evolved as a flexural basin, resulting from the ongoing overall N-S shortening (acting since circa ~8 Ma). This tectonic setting is marked by the strengthening of the subsidence and leads to the deposition of deep marine sediments (Abad marls). Then, Messinian and post-Messinian deposits are only slightly folded (Figure 13).

## Acknowledgments

We warmly thank Georges Clauzon without whom this study would not have been achieved. He provided us a new vision of the evolution of the Sorbas basin based on thorough geomorphological and biostratigraphic researches. He could not see the achievement of this study but his memory will be forever associated to the Sorbas basin. Field investigations have been supported by the CIFRE PhD grant 584/2010 (TOTAL/UPMC). This paper is a contribution to the Projects AMEDITER ("Actions Marges" CNRS/INSU Programme), "Bassins néogènes et manteau en Méditerranée" (TerMex CNRS/INSU Programme). We are grateful to Michel Diamant (INSU/IPGP) for providing us a SCINTREX CGS-M micro-gravimeter. Geophysical interpretations were drawn using Geosoft software, and the 3-D modeling process was performed using the 3-D Geomodeller (Intrepid Geophysics) developed by the BRGM (Orléans, France). We are grateful to Guillaume Martelet (BRGM) for his help and assistance on the gravity modeling process and also to Gabriel Courrioux (BRGM-GEO) for providing us a 3-D Geomodeller licensing and for his technical support. We thank two anonymous referees for their constructive contribution to improve the paper.

## References

- Amores, L. R., J. L. Hernandez-Enrile, and J. J. Martínez-Díaz (2001), Sobre los factores relacionados con la evaluación de la peligrosidad sísmica en la región de Murcia, in *Segundo Congreso Iberoamericano de Ingeniería Sísmica*, Asociación Española de Ingeniería Sísmica, Madrid, Spain.
- Amores, L. R., J. L. Hernandez-Enrile, and J. J. Martínez-Díaz (2002), Estudio gravimétrico previo aplicado a la identificación de fallas ocultas como fuentes sismogénicas en la depresión del Guadalentín (región de Murcia), *Geogaceta*, *32*, 307–310.
- Anderson, E. M. (1942), *The Dynamics of Faulting and Dyke Formation With Application to Britain*, Oliver and Boyd, Edinburgh.
- Angelier, J. (1984), Tectonic analysis of fault slip data sets, *J. Geophys. Res.*, *89*, 5835–5848, doi:10.1029/JB089iB07p05835.
- Angelier, J. (1990), Inversion of field data in fault tectonics to obtain the regional stress: A new rapid direct inversion method by analytical means, *Geophys. J. Int.*, *103*, 363–376.
- Augier, R. (2004), Evolution tardi-orogénique des Cordilères Bétiqes (Espagne): Apports d'une étude intégrée, PhD thesis, Université Pierre et Marie Curie, Paris.
- Augier, R., L. Jolivet, and C. Robin (2005a), Late Orogenic doming in the eastern Betic Cordilleras: Final exhumation of the Nevado-Filabride complex and its relation to basin genesis, *Tectonics*, *24*, TC4003, doi:10.1029/2004TC001687.
- Augier, R., P. Agard, P. Monié, L. Jolivet, C. Robin, and G. Booth-Rea (2005b), Exhumation, doming and slab retreat in the Betic Cordillera (SE Spain): In situ  $^{40}\text{Ar}/^{39}\text{Ar}$  ages and P–T–d–t paths for the Nevado-Filabride complex, *J. Metamorph. Geol.*, *23*, 357–381.
- Augier, R., L. Jolivet, D. Do Couto, and F. Negro (2013), From ductile to brittle, late- to post-orogenic evolution of the Betic Cordillera: Structural insights from the north-eastern Internal Zones, *Bull. Soc. Geol. Fr.*, *184*(4–5), 405–425.
- Azañón, J. M., and A. Crespo-Blanc (2000), Exhumation during a continental collision inferred from the tectonometamorphic evolution of the Alpujarride Complex in the central Betics (Alboran Domain, SE Spain), *Tectonics*, *19*, 549–565, doi:10.1029/2000TC900005.
- Behr, W. M., and J. P. Platt (2012), Kinematic and thermal evolution during two-stage exhumation of a Mediterranean subduction complex, *Tectonics*, *31*, TC4025, doi:10.1029/2012TC003121.
- Booth-Rea, G., J. M. Azañón, and V. García-Dueñas (2004a), Extensional tectonics in the northeastern Betics (SE Spain): Case study of extension in a multilayered upper crust with contrasting rheologies, *J. Struct. Geol.*, *26*, 2039–2058.
- Booth-Rea, G., J. M. Azañón, A. Azor, and V. García-Dueñas (2004b), Influence of strike-slip fault segmentation on drainage evolution and topography. A case study: The Palomares Fault Zone (southeastern Betics, Spain), *J. Struct. Geol.*, *26*, 1615–1632.
- Bourillot, R., E. Vennin, J. M. Rouchy, C. Durlot, V. Rommevaux, C. Kolodka, and F. Knap (2009), Structure and evolution of a Messinian mixed carbonate-siliciclastic platform: The role of evaporites (Sorbas basin, south-east Spain), *Sedimentology*, *57*, 477–512.
- Braga, J. C., J. M. Martín, and C. Quesada (2003), Patterns and average rates of late Neogene–Recent uplift of the Betic Cordillera, SE Spain, *Geomorphology*, *50*, 3–26.
- Braga, J. C., D. Bassi, J. M. Martín, R. Riding, J. Aguirre, I. M. Sánchez-Almazo, and J. Dinarès-Turell (2006), Testing models for the Messinian salinity crisis: The Messinian record in Almería, SE Spain, *Sediment. Geol.*, *188–189*, 131–154.
- Briand, M., C. Montenat, and P. Ott d'Estevou (1990), Le bassin de Huercal-Overa, in *Les bassins Néogènes du domaine Bétiq Oriental (Espagne)*, Documents et Travaux IGAL, vol. 12–13, edited by C. Montenat, pp. 239–259, Inst. Géol. Albert-de-Lapparent, Paris.
- Calcagno, P., J. P. Chilès, G. Courrioux, and A. Guillen (2008), Geological modelling from field data and geological knowledge: Part I. Modelling method coupling 3D potential-field interpolation and geological rules, *Phys. Earth Planet. Int.*, *171*(1–4), 147–157.
- CIESM (2008), The Messinian salinity crisis from mega-deposits to microbiology—A consensus report, N°33, in *CIESM Workshop Monographs*, edited by F. Briand, 168 pp., Monaco.
- Clauzon, G., J. Suc, F. Gautier, A. Berger, and M. F. Loutre (1996), Alternate interpretation of the Messinian salinity crisis: Controversy resolved?, *Geology*, *24*, 363–366.
- Cloetingh, S., A. van der Beek, D. van Rees, T. B. Roep, C. Biermann, and R. A. Stephenson (1992), Flexural interaction and the dynamics of Neogene extensional basin formation in the Alboran-Betic region, *Geo. Mar. Lett.*, *12*, 66–75.
- Comas, M. C., J. Platt, J. I. Soto, and A. B. Watts (1999), The origin and tectonic history of the Alboran basin: Insights from leg 161 results, *Ocean Drill. Program*, *161*, 555–580.
- Crespo-Blanc, A. (1995), Interference pattern of extensional fault systems: A case study of the Miocene rifting of the Alboran basement (North of Sierra Nevada, Betic Chain), *J. Struct. Geol.*, *17*, 1559–1569.
- Crespo-Blanc, A., and D. Frizon de Lamotte (2006), Structural evolution of the external zones derived from the Flysch trough and the South Iberian and Maghreb paleomargins around the Gibraltar Arc: A comparative study, *Bull. Soc. Geol. Fr.*, *177*, 267–282.
- Crespo-Blanc, A., M. Orozco, and V. García-Dueñas (1994), Extension versus compression during the Miocene tectonic evolution of the Betic Chain. Late folding of normal fault systems, *Tectonics*, *13*, 78–88, doi:10.1029/93TC02231.
- de Jong, K. (1991), Tectono-metamorphic studies and radiometric dating in the Betic Cordilleras (SE Spain) with implications for the dynamics of extension and compression in the western Mediterranean Area, PhD thesis, Vrije Univ., Amsterdam.
- de Jong, K. (2003), Very fast exhumation of high-pressure metamorphic rocks with excess  $^{40}\text{Ar}$  and inherited  $^{87}\text{Sr}$ , Betic Cordilleras, southern Spain, *Lithos*, *70*, 91–110.
- de Larouzière, F. D., J. Bolze, P. Bordet, J. Hernandez, C. Montenat, and P. Ott d'Estevou (1988), The Betic segment of the lithospheric Trans-Alboran shear zone during the late Miocene, *Tectonophysics*, *152*, 41–52.
- Díaz, J., and J. Gallart (2009), Crustal structure beneath the Iberian Peninsula and surrounding waters: A new compilation of deep seismic sounding results, *Phys. Earth Planet. Int.*, *173*(1–2), 181–190.
- Dronkert, H. (1976), Late Miocene evaporites in the Sorbas basin and adjoining areas, *Mem. Soc. Geol. Italiana*, *16*, 341–361.
- Faccenna, C., and T. W. Becker (2010), Shaping mobile belts by small-scale convection, *Nature*, *465*(7298), 602–605.
- Faccenna, C., M. Mattei, R. Funicello, and L. Jolivet (1997), Styles of back-arc extension in the central Mediterranean, *Terra Nova*, *9*, 126–130.
- Faccenna, C., C. Piromallo, A. Crespo-Blanc, L. Jolivet, and F. Rossetti (2004), Lateral slab deformation and the origin of the western Mediterranean arcs, *Tectonics*, *23*, TC1012, doi:10.1029/2002TC001488.
- Frizon de Lamotte, D., C. Raulin, N. Mouchot, J. C. Wrobel-Daveau, C. Blanpied, and J. C. Ringenbach (2011), The southernmost margin of the Tethys realm during the Mesozoic and Cenozoic: Initial geometry and timing of the inversion processes, *Tectonics*, *30*, TC3002, doi:10.1029/2010TC002691.
- Fullea, J., M. Fernandez, and H. Zeyen (2006), Lithospheric structure in the Atlantic–Mediterranean transition zone (southern Spain, northern Morocco): A simple approach from regional elevation and geoid data, *C. R. Geosciences*, *338*, 140–151.
- Fullea, J., M. Fernández, J. C. Afonso, J. Vergés, and H. Zeyen (2010), The structure and evolution of the lithosphere–asthenosphere boundary beneath the Atlantic–Mediterranean transition region, *Lithos*, *120*(1–2), 74–95.
- Galindo-Zaldívar, J., F. González-Lodeiro, and A. Jabaloy (1989), Progressive extensional shear structures in a detachment contact in the western Sierra Nevada (Betic Cordilleras, Spain), *Geodin. Acta*, *3*, 73–85.

- Galindo-Zaldívar, J., J. A. Gil, M. J. Borque, F. González-Lodeiro, A. Jabaloy, C. Marín-Lechado, P. Ruano, and C. Sanz de Galdeano (2003), Active faulting in the internal zones of the central Betic Cordilleras (SE, Spain), *J. Geodyn.*, *36*, 239–250.
- García Monzón, G., and W. Kampschuur (1972), Mapa geológico de España, Hoja 1014, Vera, Instituto Geológico y Minero de España (IGME), Ministerio de Industria y Energía, Madrid, scale 1:50000.
- García Monzón, G., W. Kampschuur, and R. L. M. Vissers (1973a), Mapa geológico de España, Hoja 1013, Macael, Instituto Geológico y Minero de España (IGME), Ministerio de Industria y Energía, Madrid, scale 1:50000.
- García Monzón, G., W. Kampschuur, R. L. M. Vissers, J. Verburg, and R. Wolff (1973b), Mapa geológico de España, Hoja 1030, Tabernas, Instituto Geológico y Minero de España (IGME), Ministerio de Industria y Energía, Madrid, scale 1:50000.
- García Monzón, G., W. Kampschuur, and J. Verburg (1974), Mapa geológico de España, Hoja 1031, Sorbas, Instituto Geológico y Minero de España (IGME), Ministerio de Industria y Energía, Madrid, scale 1:50000.
- García-Dueñas, V., J. M. Martínez-Martínez, M. Orozco, and J. I. Soto (1988), Plis-nappes, cisaillements syn- à post-métamorphiques et cisaillements ductiles-fragiles en distension dans les Nevado-Filabrides (Cordillères bétiques, Espagne), *C. R. Acad. Sci.*, *307*, 1389–1395.
- García-Dueñas, V., J. C. Balanyá, and J. M. Martínez-Martínez (1992), Miocene extensional detachments in the outcropping basement of the northern Alboran basin (Betics) and their tectonic implications, *Geo-Mar. Lett.*, *12*, 88–95.
- Giaconia, F., G. Booth-Rea, J. M. Martínez-Martínez, J. M. Azanon, J. V. Pérez-Peña, J. Pérez-Romero, and I. Villegas (2012a), Geomorphic evidence of active tectonics in the Sierra Alhamilla (eastern Betics, SE Spain), *Geomorphology*, *145*, 90–106, doi:10.1016/j.geomorph.2011.12.043.
- Giaconia, F., G. Booth-Rea, J. M. Martínez-Martínez, J. M. Azañón, and J. Pérez-Peña (2012b), Geomorphic analysis of the Sierra Cabrera, an active pop-up in the constrictional domain of conjugate strike-slip faults: The Palomares and Polopos Fault Zones (eastern Betics, SE Spain), *Tectonophysics*, *580*, 27–42, doi:10.1016/j.tecto.2012.08.028.
- Giaconia, F., G. Booth-Rea, M. J. Martínez-Martínez, M. J. Azañón, J. Pérez-Romero, and I. Villegas (2013), Mountain front migration and drainage captures related to fault segment linkage and growth: The Polopos transpressive fault zone (southeastern Betics, SE Spain), *J. Struct. Geol.*, *46*, 76–91.
- Goubert, E., D. Néraudeau, J. M. Rouchy, and D. Lacour (2001), Foraminiferal record of environmental changes: Messinian of the Los Yesos area (Sorbas Basin, SE Spain), *Palaeogeogr. Palaeoclimatol. Palaeoecol.*, *175*, 61–78.
- Gracia, E., et al. (2006), Active faulting offshore SE Spain (Alboran Sea): Implications for earthquake hazard assessment in the Southern Iberian Margin, *Earth Planet. Sci. Lett.*, *241*(3–4), 734–749.
- Guillen, A., P. Calcagno, G. Courrioux, A. Joly, and P. Ledru (2008), Geological modelling from field data and geological knowledge: Part II. Modelling validation using gravity and magnetic data inversion, *Phys. Earth Planet. Int.*, *171*(1–4), 158–169.
- Hammer, S. (1939), Terrain corrections for gravimeter stations, *Geophysics*, *4*, 184–194.
- Haq, B. U., J. Hardenbol, and R. Vail (1987), Chronology of fluctuating sea levels since the Triassic, *Science*, *235*, 1156–1167.
- Haughton, P. (2000), Evolving turbidite systems on a deforming basin floor, Tabernas, SE Spain, *Sedimentology*, *47*, 497–518.
- Haughton, P. (2001), Contained turbidites used to track sea bed deformation and basin migration, Sorbas basin, south-east Spain, *Basin Res.*, *13*, 117–139.
- Hodgson, D. M., and P. Haughton (2004), Impact of syndepositional faulting on gravity current behaviour and deep-water stratigraphy: Tabernas-Sorbas basin, SE Spain, in *Confined Turbidite Systems*, edited by S. A. Lomas and P. Joseph, pp. 135–158, Geol. Soc., London.
- Iribarren, L., J. Vergés, and M. Fernández (2009), Sediment supply from the Betic-Rif orogen to basins through Neogene, *Tectonophysics*, *475*, 68–84.
- Jabaloy, A., J. Galindo-Zaldívar, and F. González-Lodeiro (1992), The Mecina Extensional System: Its relation with the post-Aquitania piggy-back basins and the paleostresses evolution (Betic Cordilleras, Spain), *Geo-Mar. Lett.*, *12*, 96–103.
- Jacoby, W., and L. Smilde (Eds.) (2009), *Gravity Interpretation*, Germany, Springer, Heidelberg.
- Johnson, C., N. Harbury, and A. J. (1997), The role of extension in the Miocene denudation of the Nevado-Filabride Complex, Betic Cordillera (SE Spain), *Tectonics*, *16*, 189–204, doi:10.1029/96TC03289.
- Jolivet, L., and C. Faccenna (2000), Mediterranean extension and the Africa-Eurasia collision, *Tectonics*, *19*(6), 1095–1106, doi:10.1029/2000TC900018.
- Jolivet, L., R. Augier, C. Robin, J. Suc, and J. M. Rouchy (2006), Lithospheric-scale geodynamic context of the Messinian salinity crisis, *Sediment. Geol.*, *188–189*, 9–33.
- Jolivet, L., R. Augier, C. Faccenna, F. Negro, G. Rimmele, P. Agard, C. Robin, F. Rossetti, and A. Crespo-Blanc (2008), Subduction, convergence and the mode of backarc extension in the Mediterranean region, *Bull. Soc. Geol. Fr.*, *179*, 525–550.
- Joly, A., M. Faure, G. Martelet, and Y. Chen (2009), Gravity inversion, AMS and geochronological investigations of syntectonic granitic plutons in the southern part of the Variscan French Massif Central, *J. Struct. Geol.*, *31*, 421–443.
- Jonk, R., and C. Biermann (2002), Deformation in Neogene sediments of the Sorbas and Vera Basins (SE Spain): Constraints on simple-shear deformation and rigid body rotation along major strike-slip faults, *J. Struct. Geol.*, *24*, 963–977.
- Kleverlaan, K. (1989), Neogene history of the Tabernas basin (SE Spain) and its Tortonian submarine fan development, *Geol. Mijnbouw*, *68*, 421–432.
- Krijgsman, W., F. J. Hilgent, I. Raffi, F. J. Sierro, and D. S. Wilson (1999), Chronology, causes and progression of the Messinian salinity crisis, *Nature*, *400*, 652–655.
- Krijgsman, W., A. R. Fortuin, F. J. Hilgen, and F. J. Sierro (2001), Astrochronology for the Messinian Sorbas basin (SE Spain) and orbital (precessional) forcing for evaporite cyclicity, *Sediment. Geol.*, *140*, 43–60.
- Lefort, J. P., and B. N. Agarwal (1999), Of what is the center of the Ibero-Armorican arc composed?, *Tectonophysics*, *302*, 71–81.
- Li, Q., P. Ruano, A. Pedrera, and J. Galindo-Zaldívar (2012), Estructura de la cuenca sedimentaria de Tabernas-Sorbas mediante prospección gravimétrica y magnética (Zonas Internas, Cordillera Bética Oriental), *Geogaceta*, *52*, 117–120.
- Loneragan, L., and J. Platt (1995), The Malaguide-Alpujarride boundary: A major extensional contact in the Internal Zone of the eastern Betic Cordillera, SE Spain, *J. Struct. Geol.*, *17*, 1655–1671.
- Loneragan, L., and N. White (1997), Origin of the Betic-Rif mountain belt, *Tectonics*, *16*(3), 504–522, doi:10.1029/96TC03937.
- López Sánchez-Vizcaino, V., D. Rubatto, M. T. Gómez-Pugnaire, V. Trommsdorff, and O. Müntener (2001), Middle Miocene high-pressure metamorphism and fast exhumation of the Nevado-Filabride complex, SE Spain, *Terra Nova*, *13*, 327–332.
- Manzi, V., R. Gennari, F. Hilgen, W. Krijgsman, S. Lugli, M. Roveri, and F. J. Sierro (2013), Age refinement of the Messinian salinity crisis onset in the Mediterranean, *Terra Nova*, *25*(4), 315–322.
- Martelet, G. (1999), Modélisation de la structure crustale et du comportement mécanique de la lithosphère à partir des anomalies gravimétriques, Applications à l'Himalaya et au massif granitique du Mont Lozère, Cévennes, PhD thesis, Institut de Physique du Globe, Paris.
- Martelet, G., N. Debeglia, and C. Truffert (2002), Updating and validating the French gravity terrain corrections out to a distance of 167 km, *C. R. Geosci.*, *334*(7), 449–454.
- Martelet, G., P. Calcagno, C. Gumiaux, C. Truffert, A. Bitri, D. Gapais, and J. P. Brun (2004), Integrated 3D geophysical and geological modeling of the Hercynian suture zone in the Champtoceaux area (south Brittany, France), *Tectonophysics*, *382*, 117–128.

- Martín, J. M., J. C. Braga, and I. M. Sánchez-Almazo (1999), The Messinian record of the outcropping marginal Alboran basin deposits: Significance and implications, in *Proceedings of the Ocean Drilling Program, College Station, TX, Sci. Results*, vol. 161, pp. 543–551.
- Martínez-Martínez, J. M. (1985), Las Sucesiones Nevado-Filábrides en la Sierra de los Filabres y Sierra Nevada, *Cuadernos de Geología Ibérica*, 12, 127–144.
- Martínez-Martínez, J. M., and J. M. Azañón (1997), Mode of extensional tectonics in the southeastern Betics (SE Spain): Implications for the tectonic evolution of the peri-Alboran orogenic system, *Tectonics*, 16(2), 205–225, doi:10.1029/97TC00157.
- Martínez-Martínez, J. M., J. I. Soto, and J. C. Balanyá (2002), Orthogonal folding of extensional detachments: Structure and origin of the Sierra Nevada elongated dome (Betics, SE Spain), *Tectonics*, 21(3), TC001283, doi:10.1029/2001TC001283.
- Martínez-Martínez, J. M., J. I. Soto, and J. C. Balanyá (2004), Elongated domes in extended orogens: A mode of mountain uplift in the Betics (southeast Spain), in *Gneiss Domes in Orogeny*, edited by D. Whitney, C. Teysier, and C. S. Siddoway, *Geol. Soc. Am. Spec. Pap.*, 380, 243–265.
- Martínez-Martínez, J. M., G. Booth-Rea, J. M. Azañón, and F. Torcal (2006), Active transfer fault zone linking a segmented extensional system (Betics, southern Spain): Insight into heterogeneous extension driven by edge delamination, *Tectonophysics*, 422, 159–173.
- Martin-Suárez, E., M. Freudenthal, W. Krijgsman, and A. Rutgers Fortuin (2000), On the age of the continental deposits of the Zorreras Member (Sorbas basin, SE Spain), *Geobios*, 33, 505–512.
- Mather, A. E. (2000), Adjustment of a drainage network to capture induced base-level change: An example from the Sorbas basin, SE Spain, *Geomorphology*, 34, 271–289.
- Mauffret, A., A. Maldonado, and A. C. Campillo (1992), Tectonic framework of the eastern Alboran and western Algerian basins, western Mediterranean, *Geo-Mar. Lett.*, 12, 104–110.
- Meijninger, B. (2006), Late-orogenic extension and strike-slip deformation in the Neogene of southeastern Spain, PhD thesis, n°269, Universiteit Utrecht, Utrecht.
- Meijninger, B. M. L., and R. L. M. Vissers (2006), Miocene extensional basin development in the Betic Cordillera, SE Spain revealed through analysis of the Alhama de Murcia and Crevillente Faults, *Basin Res.*, 18, 547–571.
- Miller, K. G., M. A. Komins, J. Browning, J. D. Wright, G. S. Mountain, M. E. Katz, J. Sugarman, B. S. N. Christie-Blick, and S. F. Pekar (2005), The Phanerozoic record of global sea-level change, *Science*, 310, 1293–1298.
- Monié, P., and C. Chopin (1991),  $^{40}\text{Ar}$ - $^{39}\text{Ar}$  ages through high-pressure low-temperature metamorphism in the Western Alps, *Eur. J. Mineral.*, 2, 343–361.
- Monié, P., R. L. Torres-Roldán, and A. García-Casco (1994), Cooling and exhumation of the Western Betic Cordilleras,  $^{40}\text{Ar}$ / $^{39}\text{Ar}$  thermochronological constraints on a collapsed terrane, *Tectonophysics*, 238, 353–379.
- Montenat, C., and P. Ott d'Estevou (1977), Présence du Pliocène marin dans le bassin de Sorbas (Espagne méridionale), Conséquences paléogéographiques et tectoniques, *C.R. somm. Soc. Geol. Fr.*, 4, 209–211.
- Montenat, C., P. Ott d'Estevou, J. C. Plaziat, and J. Chapel (1980), La signification des faunes marines contemporaines des évaporites messiniennes dans le Sud-Est de l'Espagne. Conséquences pour l'interprétation des conditions d'isolement de la Méditerranée occidentale, *Geol. Méditerr.*, 7, 81–90.
- Montenat, C., P. Ott d'Estevou, and P. Masse (1987), Tectonic-sedimentary characters of the Betic Neogene basins evolving in a crustal transcurrent shear zone (SE Spain), *Bull. C. R. Explo. Prod. Elf-Aquitaine*, 11, 1–22.
- Ott d'Estevou, P., and C. Montenat (1990), Le bassin de Sorbas-Tabernas, in *Les bassins Néogènes du domaine Bétique Oriental (Espagne)*, Documents et Travaux IGAL, vol. 12–13, edited by C. Montenat, pp. 101–128, Inst. Géol. Albert-de-Lapparent, Paris.
- Ott d'Estevou, P., G. Termier, and H. Termier (1981), La spongiofaune Néogène de Sorbas (Andalousie orientale, Espagne), *Geol. Méditerr.*, 8(2), 61–78.
- Ott d'Estevou, P., C. Montenat, and J.-C. Alvaro (1990), Le bassin de Vera-Garrucha, in *Les bassins Néogènes du domaine Bétique Oriental (Espagne)*, Documents et Travaux IGAL, vol. 12–13, edited by C. Montenat, pp. 165–187, Inst. Géol. Albert-de-Lapparent, Paris.
- Pedraza, A., J. Galindo-Zaldívar, A. Ruiz-Constán, C. Duque, C. Marín-Lechado, and I. Serrano (2009), Recent large fold nucleation in the upper crust: Insight from gravity, magnetic, magnetotelluric and seismicity data (Sierra de Los Filabres–Sierra de Las Estancias, Internal Zones, Betic Cordillera), *Tectonophysics*, 463, 145–160.
- Pedraza, A., J. Galindo-Zaldívar, A. Tello, and C. Marín-Lechado (2010), Intramontane basin development related to contractional and extensional structure interaction at the termination of a major sinistral fault: The Huércal-Overa Basin (eastern Betic Cordillera), *J. Geodyn.*, 49, 271–286.
- Pedraza, A., J. Galindo-Zaldívar, F. Lamas, and A. Ruiz-Constán (2012), Evolution of near-surface ramp-flat-ramp normal faults and implication during intramontane basin formation in the eastern Betic Cordillera (the Huércal-Overa Basin, SE Spain), *Tectonics*, 31, TC4024, doi:10.1029/2012TC003130.
- Platt, J., and R. L. M. Vissers (1989), Extensional collapse of thickened continental lithosphere: A working hypothesis for the Alboran Sea and Gibraltar Arc, *Geology*, 17, 540–543.
- Platt, J., B. Van Den Eeckhout, E. Janzen, G. Konert, O. J. Simon, and R. Weijermars (1983), The structure and tectonic evolution of the Aguilón fold-nappe, Sierra Alhama, Betic Cordilleras, SE Spain, *J. Struct. Geol.*, 5(5), 519–538.
- Platt, J., S. Allerton, A. I. Kirker, C. Mandeville, A. Mayfield, E. Platzman, and A. Rimi (2003), The ultimate arc: Differential displacement, oroclinal bending, and vertical axis rotation in the External Betic-Rif arc, *Tectonics*, 22(3), 1017, doi:10.1029/2001TC001321.
- Platt, J., S. Kelley, A. Carter, and M. Orozco (2005), Timing of tectonic events in the Alpujarride Complex, Betic Cordillera, southern Spain, *J. Geol. Soc. London*, 162, 1–12.
- Platt, J. P., R. Anczkiewicz, J. I. Soto, S. P. Kelley, and M. F. Thirlwall (2006), Early Miocene continental subduction and rapid exhumation in the western Mediterranean, *Geology*, 34(11), 981–984.
- Poisson, A. M., J. L. Morel, J. Andrieux, M. Coulon, R. Wernli, and C. Guernet (1999), The origin and development of Neogene basins in the SE Betic Cordillera (SE Spain): A case study of the Tabernas-Sorbas and Huércal Overa Basins, *J. Petrol. Geol.*, 22(1), 97–114.
- Puga-Bernabéu, A., J. M. Martín, and J. C. Braga (2007), Tsunami-related deposits in temperate carbonate ramps, Sorbas Basin, southern Spain, *Sediment. Geol.*, 199, 107–127.
- Rehault, J., G. Boillot, and A. Mauffret (1984), The western Mediterranean basin geological evolution, *Mar. Geol.*, 55, 447–477.
- Riding, R., J. C. Braga, J. M. Martín, and I. M. Sánchez-Almazo (1998), Mediterranean Messinian salinity crisis: Constraints from a coeval marginal basin, Sorbas, southeastern Spain, *Mar. Geol.*, 146, 1–20.
- Riding, R., J. C. Braga, and J. M. Martín (2000), Late Miocene Mediterranean desiccation: Topography and significance of the “salinity crisis” erosion surface on-land in southeast Spain: Reply, *Sediment. Geol.*, 133, 175–184.
- Robinson, E., and C. Çoruh (1988), *Basic Exploration Geophysics*, John Wiley, New York.
- Roep, T. B., C. J. Dabrio, A. R. Fortuin, and M. D. Polo (1998), Late highstand patterns of shifting and stepping coastal barriers and washover-fans (late Messinian, Sorbas basin, SE Spain), *Sediment. Geol.*, 116, 27–56.

- Rouchy, J. M., and J. Saint-Martin (1992), Late Miocene events in the Mediterranean as recorded by carbonate-evaporite relations, *Geology*, *20*, 629–632.
- Rousset, D., R. Bayer, D. Guillon, and B. J. Edel (1993), Structure of the southern Rhine Graben from gravity and reflection seismic data (ECORS-DEKORP Program), *Tectonophysics*, *221*, 135–153.
- Roveri, M., R. Gennari, S. Lugli, and V. Manzi (2009), The terminal carbonate complex: The record of sea-level changes during the Messinian salinity crisis, *GeoActa*, *8*, 63–78.
- Ruano, P., J. Galindo-Zaldívar, and A. Jabaloy (2004), Recent tectonic structures in a transect of the central Betic Cordillera, *Pure Appl. Geophys.*, *161*, 541–563.
- Rutter, E. H., D. R. Faulkner, and R. Burgess (2012), Structure and geological history of the Carboneras Fault Zone, SE Spain: Part of a stretching transform fault system, *J. Struct. Geol.*, *42*, 227–245.
- Salcher, B. C., B. Meurers, J. Smit, K. Decker, M. Hoelzel, and M. Wagneich (2012), Strike-slip tectonics and Quaternary basin formation along the Vienna basin fault system inferred from Bouguer gravity derivatives, *Tectonics*, *31*, TC3004, doi:10.1029/2011TC002979.
- Sanchez-Almazo, I. M., J. C. Braga, J. Dinares-Turell, J. M. Martin, and B. Spiro (2007), Palaeoceanographic controls on reef deposition: The Messinian Cariatiz reef (Sorbas Basin, Almería, SE Spain), *Sedimentology*, *54*, 637–660.
- Sanz de Galdeano, C. (1985), Estructura del borde oriental de la Sierra de Gádor (zona Alpujárride, Cordilleras Béticas), *Acta Geol. Hisp.*, *20*, 145–154.
- Sanz de Galdeano, C., and J. A. Vera (1992), Stratigraphic record and palaeogeographical context of the Neogene basins in the Betic Cordillera, Spain, *Basin Res.*, *4*, 21–36.
- Sanz de Galdeano, C., S. Shanov, J. Galindo-Zaldívar, A. Radulov, and G. Nikolov (2010), A new tectonic discontinuity in the Betic Cordillera deduced from active tectonics and seismicity in the Tabernas basin, *J. Geodyn.*, *50*, 57–66.
- Sierro, F. J., J. A. Flores, J. Civis, J. A. González Delgado, and G. Francés (1993), Late Miocene globorotaliid event-stratigraphy and biogeography in the NE-Atlantic and Mediterranean, *Mar. Micropaleontol.*, *21*, 143–167.
- Spakman, W., and R. Wortel (2004), A tomographic view on western Mediterranean geodynamics, in *The TRANSMED Atlas, The Mediterranean Region From Crust to Mantle*, edited by W. Cavazza et al., pp. 31–52.
- Stapel, G., R. Moeys, and C. Biermann (1996), Neogene evolution of the Sorbas basin (SE Spain) determined by paleostress analysis, *Tectonophysics*, *255*, 291–305.
- Szafán, P., and F. Horváth (2006), Crustal structure in the Carpatho-Pannonian region: Insights from three-dimensional gravity modeling and their geodynamic significance, *Int. J. Earth Sci.*, *95*, 50–67.
- Talbot, J. Y., G. Martelet, G. Courrioux, C. Yan, and M. Faure (2004), Emplacement in an extensional setting of the Mont Lozère–Borne granitic complex (SE France) inferred from comprehensive AMS, structural and gravity studies, *J. Struct. Geol.*, *26*, 11–28.
- Telford, W. M., L. Geldart, and R. E. Sheriff (Eds.) (1990), *Applied Geophysics*, Cambridge Univ. Press, Cambridge, New York.
- Torne, M., M. Fernandez, M. C. Comas, and J. I. Soto (2000), Lithospheric structure beneath the Alboran basin: Results from 3D gravity modeling and tectonic relevance, *J. Geophys. Res.*, *105*, 3209–3228, doi:10.1029/1999JB900281.
- Torres-Roldán, R. L. (1979), The tectonic subdivision of the Betic Zone (Betic Cordilleras, southern Spain); its significance and one possible geotectonic scenario for the westernmost Alpine Belt, *Am. J. Sci.*, *279*, 19–51.
- Troelstra, S. R., H. M. van De Poel, C. H. A. Huisman, L. P. A. Geerlings, and H. Dronkert (1980), Paleocological changes in the latest Miocene of the Sorbas basin, S. E. Spain, *Geol. Méditerr.*, *7*(1), 115–126.
- Turrillot, P., M. Faure, G. Martelet, Y. Chen, and R. Augier (2011), Pluton-dyke relationships in a Variscan granitic complex from AMS and gravity modeling. Inception of the extensional tectonics in the South Armorican Domain (France), *J. Struct. Geol.*, *33*, 1681–1698.
- Vázquez, M., A. Jabaloy, L. Barbero, and F. M. Stuart (2011), Deciphering tectonic- and erosion-driven exhumation of the Nevado-Filabride Complex (Betic Cordillera, Southern Spain) by low temperature thermochronology, *Terra Nova*, *23*, 257–263.
- Vergés, J., and M. Fernández (2012), Tethys-Atlantic interaction along the Iberia-Africa plate boundary: The Betic-Rif orogenic system, *Tectonophysics*, *579*, 144–172.
- Vissers, R. L. M., J. Platt, and D. van der Wal (1995), Late orogenic extension of the Betic Cordillera and the Alboran Domain: A lithospheric view, *Tectonics*, *14*, 786–803, doi:10.1029/95TC00086.
- Watts, A. B., J. Platt, and P. Buhl (1993), Tectonic evolution of the Alboran Sea basin, *Basin Res.*, *5*, 153–177.
- Weijermars, R. (1987), The Palomares brittle-ductile Shear Zone of southern Spain, *J. Struct. Geol.*, *9*(2), 139–157.
- Weijermars, R., T. B. Roep, B. van den Eeckhout, G. Postma, and K. Kleverlaan (1985), Uplift history of a Betic fold nappe inferred from Neogene-Quaternary sedimentation and tectonics (in the Sierra Alhamilla and Almería, Sorbas and Tabernas Basins of the Betic Cordilleras, SE Spain), *Geol. Mijnbouw*, *64*, 397–411.
- Wortel, M. J. R., and W. Spakman (2000), Subduction and slab detachment in the Mediterranean-Carpathian region, *Science*, *290*, 1910–1917.
- Ziegler, A., and P. Dèzes (2006), Crustal evolution of western and central Europe, *Mem. Geol. Soc. London*, *32*, 43–56.